Cambridge Centre for Computational Chemical Engineering

University of Cambridge

Department of Chemical Engineering

Preprint ISSN 1473 – 4273

A mechanistic study on the simultaneous reduction of soot and nitric oxide from diesel engine exhaust

Abhijeet Raj [1] Markus Sander [1] Markus Kraft [1]

released: 16 September 2009

[1] Department of Chemical Engineering
University of Cambridge
New Museums Site
Pembroke Street
Cambridge, CB2 3RA
UK
E-mail: mk306@cam.ac.uk

Preprint No. 83

c4e

Key words and phrases: DFT, PAH, soot, NOx, aromatic site, kinetic Monte-Carlo, simulation, modelling

Edited by
Cambridge Centre for Computational Chemical Engineering
Department of Chemical Engineering
University of Cambridge
Cambridge CB2 3RA
United Kingdom.

Fax: + 44 (0)1223 334796
E-Mail: c4e@cheng.cam.ac.uk
World Wide Web: http://www.cheng.cam.ac.uk/c4e/

Abstract

In this paper, the non-catalytic interaction between soot and nitric oxide (NO) for their simultaneous reduction is studied on different types of reactive sites that can be present on soot. The reaction mechanism proposed in our previous work [Sander *et al.*, Carbon, 47:866-875, 2009] has been extended by including seven newly proposed reaction pathways. The energetics and the kinetics of the new reactions are studied using density functional theory (DFT) and transition state theory, respectively, and their evaluated rates are presented. Due to a discrepancy in the rate for CO removal from soot surface in the literature, a new rate for it is suggested. A Polycyclic Aromatic Hydrocarbon (PAH) model, referred to as the kinetic Monte Carlo–Aromatic Site (KMC-ARS) model is used to simulate the reaction between NO and soot to form CO, N_2 and N_2O. The simulation results are compared to the experimental findings both qualitatively and quantitatively. A satisfactory agreement between them is obtained with the newly proposed rate for CO removal. The reaction between NO and soot is found to depend strongly on the type of sites present on soot, and the reaction temperature. For a set of temperatures, computed structures of PAHs are analysed to determine the functional groups present on PAHs, which are responsible for the decrease in soot reactivity towards NO with increasing reaction time. The interaction between NO and soot in isothermal conditions reveals that with increasing temperature, the number of O atoms remaining on soot surface decreases, and the number of N atoms increases for a given reaction time.

Contents

1 Introduction

Soot particles and NO_x molecules, present in the exhaust from diesel engines and other combustion devices, are known to be hazardous to human health and environment. Upon inhalation, soot particles can cause cancer, asthma and cardiac problems [23]. Continuous exposure to nitric oxide, NO, which is present in highest concentration among all the NO_x molecules can lead to tissue toxicity and renal diseases [3, 22]. NO molecules, being highly reactive, are also involved in the depletion of ozone layer, and in causing photochemical smog and acid rain. Therefore, it is necessary to work towards the reduction or, if possible, complete removal of these pollutants from the exhaust gases.

Recently, a wide variety of work, both experimental as well as theoretical, has been conducted in order to reduce the formation of soot and NO_x [1, 12, 14, 44]. For NO_x molecules, most of the suggested methods involve post-combustion gas treatment to trap them or convert them into N_2 and O_2/H_2O, and are briefly listed below. Zeolite and activated carbon [56] have been suggested for absorbing NO_x molecules at low temperatures (< 500 K). At high temperatures, NO can be desorbed from zeolite, or can be converted to N_2 and CO on activated carbon with or without the use of catalysts [1]. One of the most popular techniques to reduce NO_x is Selective Catalytic Reduction (SCR) [5, 19, 47]. This method requires a catalyst (for example, V_2O_5) and a reducing agent (for example, urea or NH_3) for the conversion of NO_x to N_2 and H_2O. NH_3 reacts with OH on the surface of catalysts to form an NH_2 radical, which, on reaction with NO, forms N_2 and H_2O. The NH_2 radical forms at high temperatures, and therefore this method has a very narrow temperature range of applicability. A low-cost method, which does not require catalysts, is also suggested in the literature: Selective Non-Catalytic Reduction (SNCR) [19, 47]. In this method, NH_3 is allowed to interact with the exhaust gas as soon as the gas leaves the engine, when the temperature is very high. However, a low conversion of NO_x to N_2 and H_2O by NH_3 is obtained possibly due to low mixing [31]. The three-way catalytic converters effectively convert CO to CO_2, hydrocarbons to CO_2 and H_2O, and NO_x to N_2 and O_2 in gasoline engines [47]. However, these converters do not perform well for NO_x in the presence of O_2, especially when the concentration O_2 is $> 2\%$. In a diesel exhaust, about 10% O_2 is present, which significantly decreases their ability to reduce NO_x. Exhaust gas recirculation (EGR) in engines can reduce the formation of NO_x by decreasing the combustion temperature. However, this method also has a limited usage, as it increases the formation of soot while reducing NO_x [59].

The above mentioned techniques focussed on NO_x reduction. For capturing the particulate matter, or soot, a diesel particulate filter (DPF) in the exhaust pipeline is used, which has an efficiency of over 99% [55]. However, such filters require periodic regeneration to avoid pressure build-up in the exhaust pipe when their pores are clogged. The most economical way to regenerate them would be to oxidise soot using NO_x and O_2, as they are already present in the engine exhaust. However, the temperature of these gases are relatively low (≈ 300°C) as compared to the temperature inside engines. This makes the non-catalytic oxidation of soot difficult to achieve. To enhance its oxidation rate, several methods have been suggested. For example, using oxidation catalysts in the DPFs to burn unburnt fuel and hydrocarbons present in the engine exhaust, and thus raising the soot temperature, can accelerate its oxidation process [43]. Also, Pt and BaO based catalysts,

which are very efficient NO carriers (through the formation of nitrates on their surface), can capture NO and release it later, when required, to oxidise soot [34]. Generally, layers of catalysts are placed on the DPFs to enhance the oxidation rate of trapped soot. The catalysts help in the soot oxidation by fixing elemental O atoms on the soot surface from O_2 present in the gas-phase (for example, Fe_2O_3 [38]). Several studies are present in the literature on catalytic oxidation of soot by NO_x and O_2 [25, 32, 38]. However, the role of the catalyst is not very well understood. To investigate this, experimental studies were conducted in [34, 38]. It was found that the catalysts are mainly involved in elemental O addition on soot. They are not directly involved in CO/CO_2 removal from soot, NO_x addition on soot, or in the formation of N_2/N_2O on the soot surface. Therefore, oxidation of soot by NO_x takes place non-catalytically.

From the studies reported above, it is clear that NO_x and O_2 are potential candidates to oxidise soot. The kinetics of soot oxidation by O_2 has been studied in detail in [9, 18, 24, 40]. However, the interaction between soot and NO_x molecules leading to the formation of N_2 and N_2O is very complex, and is not very well understood [14]. It is observed in experiments that soot–NO_x reaction stops after some time, but the reason is not clear. It is believed that this happens due to the formation of stable surface functional groups such as pyrrolic, pyridinic and pyridonic fragments, as there is evidence for the presence of such groups on soot [28, 44]. Several theoretical studies have been conducted in the past, but, a detailed mechanism showing the formation of such groups is not present in the literature. In order to accurately model the burn-out of soot in DPFs, it is necessary to improve the mechanistic understanding on the interaction between NO_x and soot to produce CO and N_2. For mechanism development, several experiments on soot oxidation by NO and NO_2 have been carried out to characterise the species being formed in the reaction, and the possible routes for their formation have been suggested [6, 7, 13, 33]. In [17], it is mentioned that the oxidation of soot by NO_2 is faster than NO. However, NO_2 is only involved in the addition of an O atom to the soot surface leading to the formation of NO in the gas-phase [16, 46]. Further oxidation of soot can then take place by NO. Therefore the study of soot oxidation by NO is important. In order to verify the proposed mechanisms through experiments, and to ensure that the intermediate species proposed in the mechanisms are stable, quantum calculations, as shown in [26, 27, 30], are required. In this direction, recently, an article was published on the theoretical study of the simultaneous reduction of soot and NO molecules [39]. Two reaction pathways along with the rates of the elementary reactions were presented. This study was restricted to the "zigzag" type of reactive site on soot particles, and a need for the mechanism extension to other types of reactive site was highlighted. The present study focusses on different reactive sites that can be present on a soot surface, and the interaction of NO molecules with them.

The purpose of this work is to present a detailed reaction mechanism depicting the interaction between NO and soot surface. The proposed reaction pathways have been studied using density functional theory (DFT). For this work, the B3LYP functional with the 6-311++G(d,p) basis set has been used for all the calculations. The reaction kinetics have been studied using transition state theory. Furthermore, a Polycyclic Aromatic Hydrocarbon (PAH) model based on a kinetic Monte Carlo algorithm has been used to study the oxidation of PAHs, which are thought to be precursors in soot formation, employing the detailed reaction mechanism. The reactions which dominate during the NO oxidation

process have been determined using this model. The resulting structures from the oxidation simulations have been analysed to determine possible reasons for the experimental observations which suggest that the reactions between soot and NO stop after a certain period of time.

2 Calculation details

The molecular structures of the stable chemical species and transition states involved in the reactions were optimised using the B3LYP hybrid functional and the 6-311++G(d,p) basis set. For the stable species, the structures were optimised with different spin multiplicities to determine the multiplicity with the minimum energy, reasonable geometry and negligible spin contamination [58]. All the DFT calculations were performed using GAUSSIAN 03 [10]. Vibrational frequencies were also calculated, and it was ensured that the stable species do not have any imaginary frequencies and the transition states have only one imaginary frequency. The vibrational mode of the imaginary frequency of all the transition states was animated to confirm that the motion correctly connects the corresponding reactants and products.

Before using B3LYP/6-311++G(d,p) level of theory for the theoretical calculations, the results obtained from the DFT calculations were validated by comparing them with experimental or theoretical data available for carbon-nitrogen-oxygen systems. Firstly, the reaction energy for the reaction $N + NO \rightarrow N_2 + O$ was evaluated using B3LYP/6-311++G(d,p), and was found to be 308 kJ/mol. This value compares very well with the literature value of 313.8 kJ/mol [2]. The reaction energy involved in the removal of a CO molecule was determined using the reaction $C_6H_5O \rightarrow C_5H_5 + CO$. A value of 127 kJ/mol was found, which agrees reasonably well with the value of 103.3 kJ/mol present in the literature [2]. Validation of DFT results with this level of theory have been published in [36] for carbon-hydrogen systems with good agreement between theory and experiment. It is clear from these comparisons that DFT accurately predicts the reaction energies for the molecular system under investigation. However, a number of studies in the literature [21, 29, 45, 48] show that the B3LYP functional under-predicts the reaction barrier heights. This under-prediction can lead to overestimates of reaction rate constants. According to the findings of [54] and Refs. therein, the error in the calculated reaction barrier introduced by density functional theory (DFT) can be as high as 5 kcal/mol. It has been shown in [36] that such an error can over-predict the rate constants by more than an order of magnitude at low temperatures ($< 700^{o}$C). Therefore, a large error in the reaction barrier is not permissible at low temperatures. The higher levels of theory, such as CCSD(T), would give more accurate barrier heights. However, these methods are prohibitively demanding on computational resources, specially for large molecules such as PAHs. To our knowledge, for the analysis of reaction mechanisms on PAHs in a reasonable computational time, DFT is the only suitable theoretical alternative to the higher levels of theory [36, 48].

The rate constants for the reactions involved in the proposed pathways were evaluated using transition state theory (TST). The partition functions for the transition state and reactants were calculated at a range of temperatures (300–3000 K) using the vibrational frequencies, moments of inertia, mass and electronic multiplicity, all of which are given

by the quantum calculations. A linear least-square fitting algorithm was used to fit the modified Arrhenius expression (equation 1) to the data points of the rate constants in order to obtain the rate coefficients A, n and E:

$$k(T) = A \times T^n \times \exp\left(\frac{-E}{RT}\right). \tag{1}$$

It is well known that transition state theory does not consider quantum tunnelling. This may lead to an under-estimation of the rate constants for the elementary reactions. To assess the role of quantum tunnelling, there are four efficient methods in the literature to evaluate the tunnelling correction factor (or, transmission constant): Wigner correction, Eckwart correction, Zero-curvature tunnelling (ZCT) correction and small curvature tunnelling (SCT) correction. The first two one-dimensional methods are mainly used for the rates calculated using TST. The curvature tunnelling methods are generally used for the rates calculated using variational transition state theory (VTST). ZCT and SCT predict the correction factor very efficiently, especially at low temperatures (T $<$ 500 K). However, at higher temperatures (T $>$ 500 K), the correction factors determined by all the methods begin to converge to similar values [4, 11]. In this work, the Wigner method was employed to obtain the tunnelling correction factors for all the elementary reactions. The correction factor, $C_W(T)$ is expressed as:

$$C_W(T) = 1 - \frac{1}{24}\left(\frac{h\nu^{\ddagger}}{k_B T}\right)^2 \tag{2}$$

where, h is Planck′s constant, k_B is Boltzmann constant, and $\nu^{\ddagger}$ is the imaginary frequency of the transition state. The rate constants are then evaluated as a product of $C_W(T)$ and $k(T)$.

3 Results and discussion

3.1 PAH–nitric oxide interaction: DFT calculations

It is well known that the chemisorption of NO on soot leads to the formation of CO, N_2 and N_2O [6]. In order to understand the mechanism for their formation, knowledge of the composition and the reactive sites of soot particles is required. Morphological studies on soot conducted using High Resolution Transmission Electron Microscopy (HRTEM) indicate that soot particles are composed largely of planar PAHs [8, 15, 49, 50]. These PAHs stack together to form parallel atomic layers, and are aligned along the periphery of soot particles. Some randomly oriented PAHs are also present in the core of soot particles [51]. Consequently the knowledge about the reaction pathways for the interaction between soot and NO can be obtained through the study of the reactivity of NO molecules towards the sites present on PAHs.

Figure 1 shows an example PAH molecule with different types of reactive sites: free-edge (FE) site formed by two carbon atoms, zigzag (ZZ) site formed by three carbon atoms,

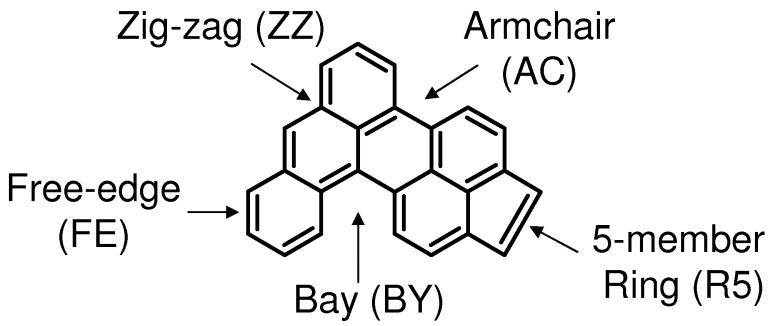

Figure 1: *An example PAH showing the principal surface site types.*

armchair (AC) site formed by four carbon atoms, and bay (BY) site formed by five carbon atoms. In our previous work [39], two reaction pathways describing the chemisorption of NO on PAHs composed of zigzag sites, and the formation CO and N_2 were presented. This work used a PAH growth model, called the kinetic Monte Carlo Aromatic Site (KMC-ARS) model, which uses a kinetic Monte Carlo algorithm to simulate PAH growth and reduction processes. A reaction mechanism for the interaction of PAHs and NO at zigzag sites was used to study their simultaneous reduction. This model was able to store the information about the structure of PAHs and their reactive sites after each reaction [35]. As observed in experiments, it was found in the simulations that the NO–PAH reaction stops after some time. Figure 2 shows an example simulated PAH structure, which could not react further with the reaction mechanism proposed in [39]. There can be two possible reasons for the reactions to stop: a) absence of reactive sites for the chemisorption of NO, or b) absence of reactions in the mechanism for the newly generated reactive sites and atoms such as embedded and surface N atoms (as shown inside circles in Figure 2), which may react further.

Assuming that the reaction mechanism is incomplete, in this paper we have explored new pathways for the formation of N_2, N_2O and CO on different types of reactive site and N atoms. As a consequence of DFT calculations on large PAHs being very computationally expensive, the smallest possible PAH model molecules fulfilling the requirements of the mechanism for each pathway have been chosen.

3.1.1 Pathway 1

Figure 3 shows the energy diagram for pathway 1. This pathway requires the presence of an armchair site in between two zigzag sites. The main purpose of choosing this site combination was to study the formation of an N_2 ring on an armchair site, and to check for the possibility of the removal of such N_2 rings from PAHs. To meet this requirement, pentaphene with four active (radical) carbon atoms (CS1) was chosen as the model molecule, as shown in Figure 3. In this pathway, firstly, two NO molecules are chemisorbed on the zigzag sites. No transition state could be obtained for this reaction. This reaction was highly exothermic with a reaction energy of 861 kJ/mol. In [39], the reaction energy for the adsorption of two NO molecules on naphthacene was reported to be 964 kJ/mol. This difference in the reaction energy indicates that the stability of NO molecules on PAHs

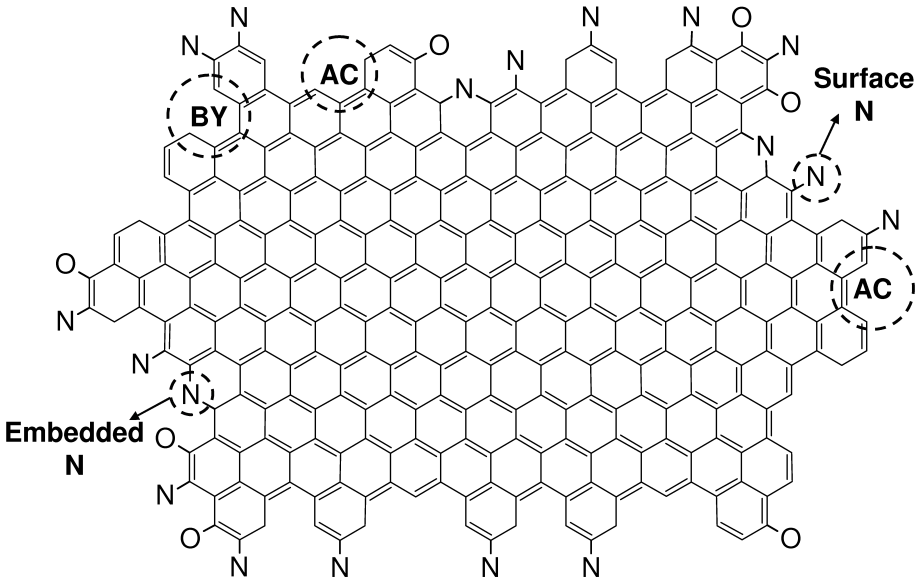

Figure 2: *An example simulated PAH structure, which cannot react further with the reaction mechanism proposed in [39]. This figure has been reproduced from [39]. Some sites on this structure are shown in circles, which may react further if reactions for those sites are included in the mechanism.*

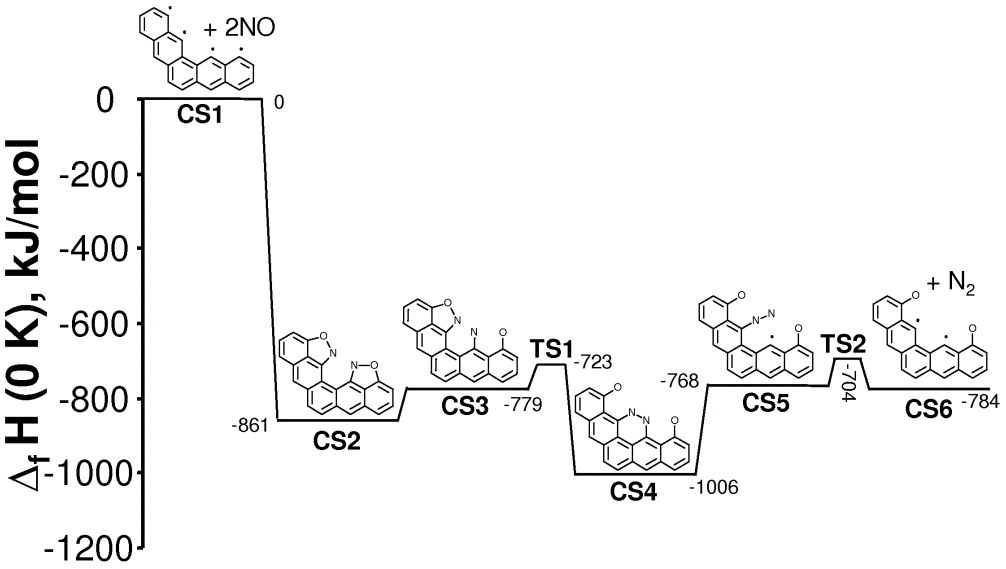

Figure 3: *Pathway 1: Potential energy diagram showing the formation of an* $\mathrm{N_2}$ *molecule on a PAH, when two* NO *molecules are chemisorbed on two zigzag sites, and the two N atoms interact on an armchair site. For PAH reactions to take place through this pathway, an armchair site in between two zigzag sites is required (fulfilled by CS1). The aim behind studying this pathway was to check the possibility of the removal of a* $\mathrm{N_2}$ *molecule adsorbed on an armchair site, as molecules adsorbed on armchair sites are very stable (discussed later).*

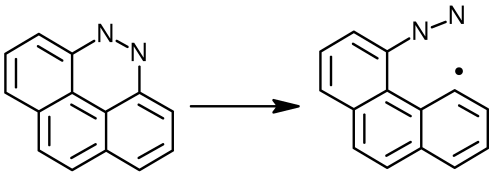

Figure 4: N_2 *ring breakage on an armchair site of a PAH molecule.*

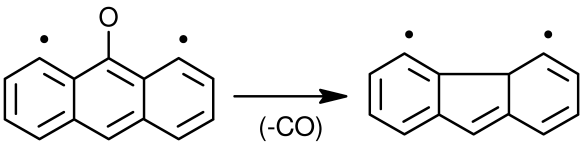

Figure 5: CO *removal from a PAH molecule.*

depends strongly on the orientation of the reactive zigzag sites. After NO chemisorption, one of the two N-O bonds on the PAH breaks. The two nearby N atoms present on the armchair site form a bond, creating the most stable species in this pathway, CS4 with a six member N_2 ring on it. Thereafter, one of the C-N bonds can break, forming an N_2 chain. This reaction is endothermic involving a reaction energy of 268 kJ/mol. For this reaction, a transition state could not be found for such a large PAH structure (CS4). Therefore, this reaction was studied on a smaller PAH, phenanthrene, as shown in Figure 4 in order to obtain the rate for this reaction. After the opening of the N_2 ring (CS5), N_2 molecule can get desorbed from the PAH. This desorption was found to be exothermic with a reaction energy of 80 kJ/mol. The remaining two O atoms can oxidise the PAH molecule through the formation of CO molecules. The removal of CO molecules from PAHs has already been studied in [9, 18, 24, 40], and hence the detailed mechanistic study of this reaction was not carried out in this work. Only one pathway for CO removal was studied in this work, as shown in Figure 5, due to reasons mentioned later in this paper. The potential energy barrier involved in this reaction was 443 kJ/mol, which matches reasonably well with the calculated values of 416 kJ/mol in [40]. The difference in these values is likely due to the use of different model molecules and different levels of theory for the quantum calculations.

3.1.2 Pathway 2

In Pathway 2, the chemisorption of NO molecules on armchair sites of a PAH molecule, and the possibility of further reactions was studied. Figure 6 shows the potential energy diagram along with the chemical species involved in this pathway. Dibenzo[a,l]tetracene with 4 active carbon atoms (CS7) was chosen as the model molecule. The addition of NO molecules on CS7 was exothermic giving an energy change of 890 kJ/mol, which is higher than the reaction energy involved in the chemisorption of NO molecules on zigzag sites in pathway 1. To ensure that the energy released in the addition of NO on armchair sites is indeed higher than that on zigzag sites, this energy was calculated on small PAHs (shown in Figure 7) to minimise the effect of the relative orientations of reactive sites (as

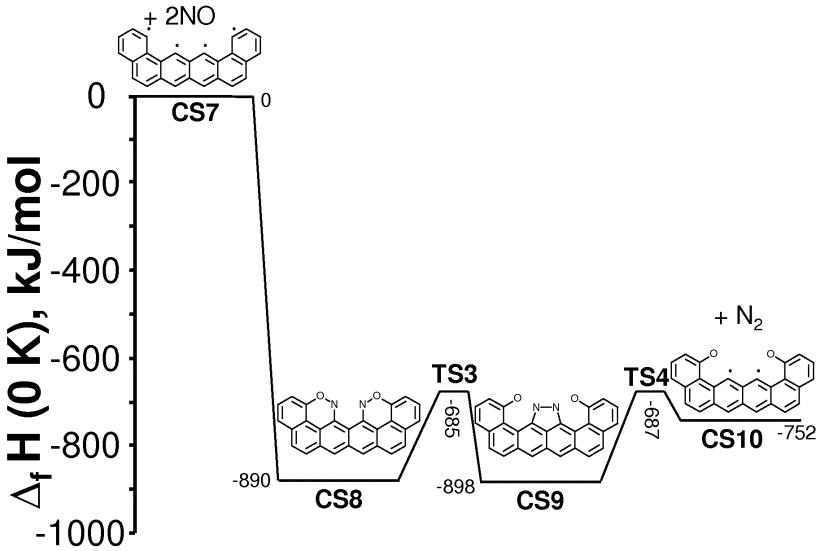

Figure 6: *Pathway 2: Potential energy diagram showing the formation of an* $\mathrm{N_2}$ *molecule on a PAH, when two* NO *molecules are chemisorbed on two armchair sites. The chemical species with one of the N-O bonds broken on an armchair site was not found to be stable. Therefore, N-N ring formation (*$\mathrm{CS8} \rightarrow \mathrm{CS9}$*) took place with the simultaneous breakage of both the N-O bonds (unlike pathway 1). For PAH reactions to take place through this pathway, a zigzag site in between two armchair sites is required (fulfilled by CS7).*

Figure 7: *Addition of* NO *on active zigzag and armchair sites of small PAHs. (a)* NO *addition on Naphthalene radical. (b)* NO *addition on Phenanthrene radical.*

stated in section 3.1.1). The reaction energy for the addition of NO on the zigzag site of Naphthalene was found to be 79 kJ/mol. This energy was 198 kJ/mol for the addition of NO on the armchair site of Phenanthrene indicating that the NO molecule forms a very stable structure on armchair sites [26]. Unlike pathway 1, this mechanism does not proceed with the breakage of one of the N-O bonds on the PAH, as the resulting molecule is not stable (geometry optimisation of the molecule with one of the N-O bonds of CS8 broken resulted in the formation of CS8 again). In this case, both the N-O bonds break simultaneously to form an N-N ring on the PAH (CS9). This reaction CS8 $\rightarrow$ CS9 is exothermic with a reaction energy of 8 kJ/mol. Thereafter, the N_2 molecule gets desorbed from the PAH. The resulting O atoms can oxidise the PAH through the formation of CO molecules.

3.1.3 Pathway 3

In pathway 3, the interaction between two NO molecules chemisorbed on a zigzag site and an armchair site was studied. Figure 8 shows the energy diagram for this pathway. Benzo[a]tetracene with four active carbon atoms (CS11) were chosen as the model molecule. Only the NO molecule present on the zigzag site undergoes N-O bond breakage, which reduces the distance between two N atoms on the PAH to facilitate N-N ring formation (CS13 $\rightarrow$ CS14). It is interesting to note that the potential energy barriers, $E^{\ddagger}$ required to be overcome for the N_2 ring formation in the pathways 1–3 follow the order: $E^{\ddagger}_{CS3\rightarrow CS4}(56\ \mathrm{kJ/mol}) < E^{\ddagger}_{CS13\rightarrow CS14}(60\ \mathrm{kJ/mol}) < E^{\ddagger}_{CS8\rightarrow CS9}(205\ \mathrm{kJ/mol})$. This shows that the presence of NO on armchair sites increases the energy required for the formation of an N_2 ring on PAHs. Thereafter, similar to pathway 1, an N_2 chain forms on the PAH, which subsequently gets desorbed. The transition state involved in the desorption of N_2 from PAH (CS15 $\rightarrow$ CS16) could not be found. Therefore, this reaction was studied on a smaller PAH molecule, as shown in Figure 9 to determine the rate for this reaction.

3.1.4 Pathway 4

Figure 10 shows the potential energy diagram along with the chemical species involved in pathway 4. As mentioned before, a large number of surface N atoms were present on the simulated PAH structure (Figure 2), and therefore, PAH reactions were required in the mechanism for their removal. The purpose of mechanism 4 is twofold: a) to present

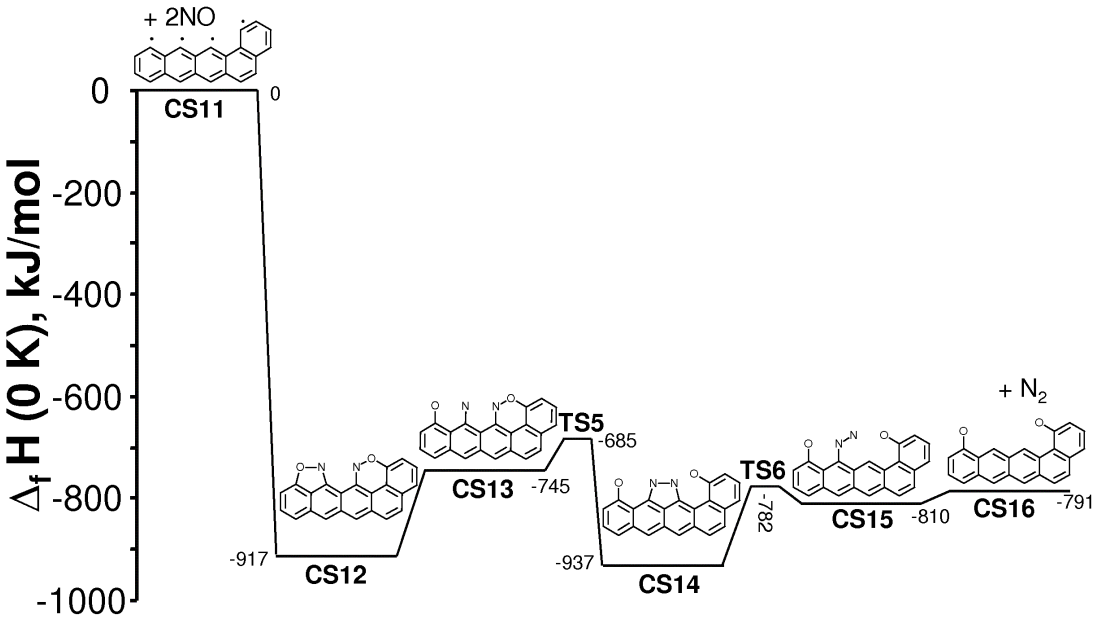

Figure 8: *Pathway 3: Potential energy diagram showing the formation of an* $\mathrm{N_2}$ *molecule on a PAH, when two* NO *molecules chemisorbed on a zigzag and an armchair site interact with each other. For PAH reactions to take place through this pathway, two consecutive zigzag sites are required next to an armchair site (fulfilled by CS11). The energy barrier required for the N-N ring formation in this pathway ((*CS13 $\rightarrow$ CS14*)) is higher than the barrier for the same reaction in pathway 1 (*CS3 $\rightarrow$ CS4*). This shows that a higher energy is required to break an N-O bond when it is present on an armchair site as compared to a zigzag site.*

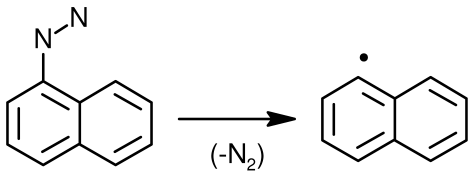

Figure 9: *Desorption of* $\mathrm{N_2}$ *chain from a PAH.*

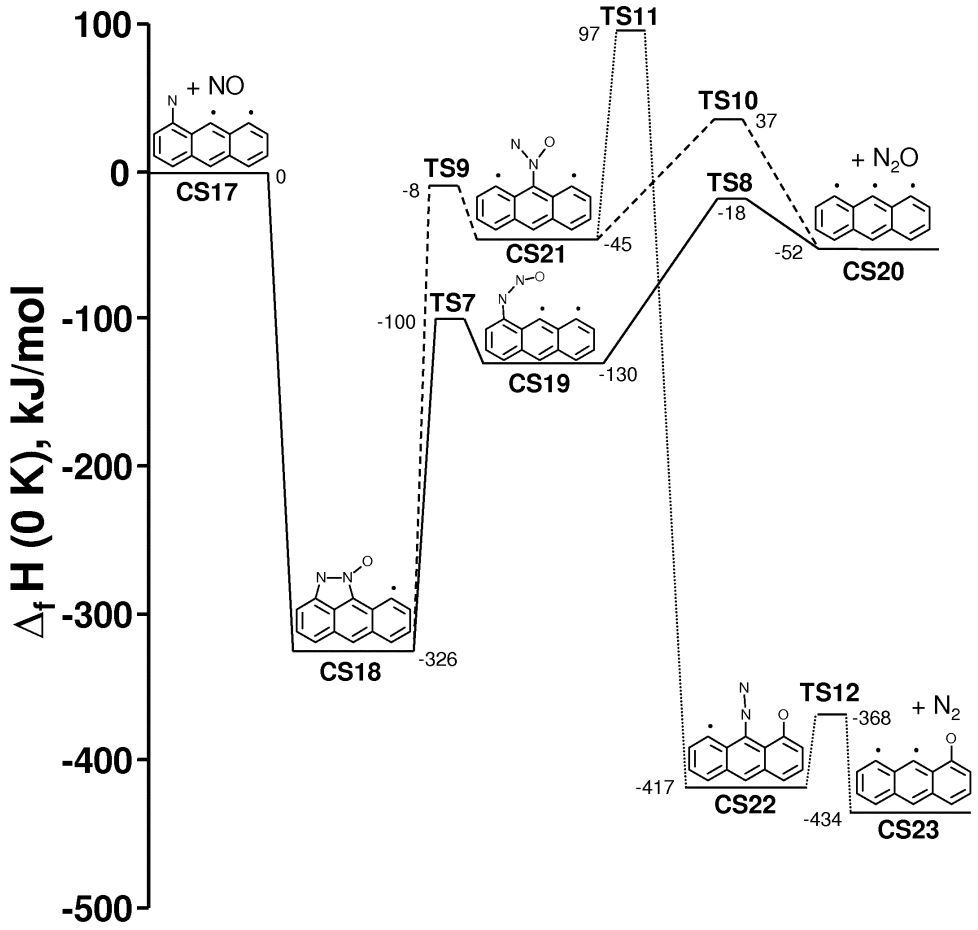

Figure 10: *Pathway 4: Potential energy diagram showing the formation of an* N_2 *and an* N_2O *from a surface N atom present on a PAH.*

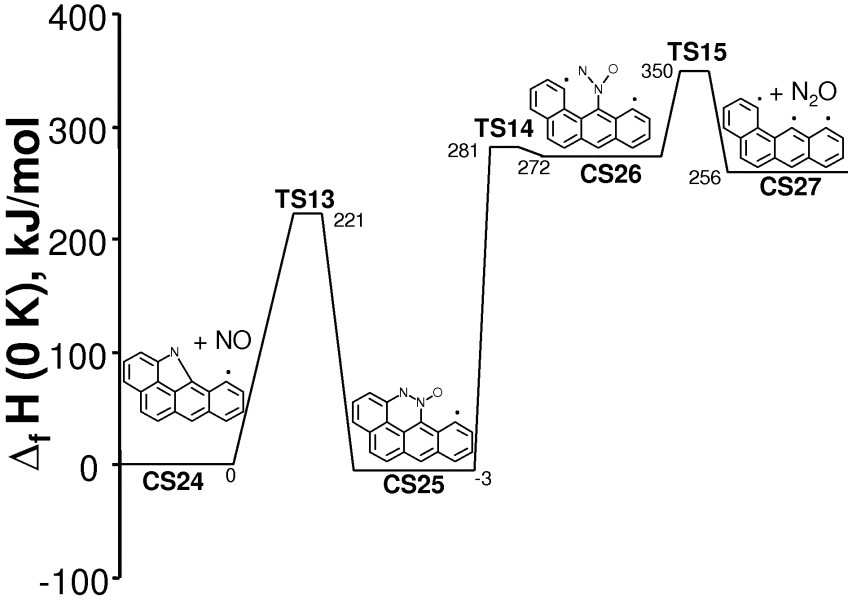

Figure 11: *Pathway 5: Potential energy diagram showing the formation of* N_2O *from embedded N atoms involved in the formation of 5-member rings on PAHs.*

the reactions that can take place on surface N atoms, and b) to propose a route for the formation of N_2O. For this mechanism, a surface N atom was required on a zigzag site. Therefore, anthracene with an N atom and two radical C atoms on it (CS17) was chosen as the model molecule. Firstly, NO chemisorption on CS17 takes place, forming a 5-member N_2O ring on the zigzag site. This type of chemisorption of NO on surface N atom is also shown in [30]. For any further reaction to take place, the energy barrier (226 kJ/mol) has to be overcome. At this stage, there can be two possible ways to break the N_2O ring, as represented by chemical species CS19 and CS21. The chain-like N_2O structure (CS19) or the branched chain-like structure (CS21) can get desorbed from the PAH, thus releasing N_2O in the gas-phase. The chemical species CS21 can also donate its O atom to a nearby active site on the PAH by overcoming a potential energy barrier of 142 kJ/mol. The molecule CS22 formed after this O-transfer is very stable, and this highly exothermic reaction has a reaction energy of 514 kJ/mol. The N_2 chain present on CS22 can get desorbed to form species CS23, which in turn can get oxidised by the O atom to release CO.

3.1.5 Pathway 5

Pathway 5, as shown in Figure 11, is very similar to pathway 4, except that this pathway requires the presence of an embedded N atom forming a five membered ring on an arm-chair site of a PAH molecule. Tetraphene with an embedded N atom and two radical C atoms on it (CS24) was chosen as the model molecule. The embedded N atom on PAH is very stable and a high energy barrier of 221 kJ/mol has to be overcome to add an NO molecule to it. This results in the formation of a 6-member N_2O ring (CS25). The breakage of this N_2O ring to form a branched N_2O chain (CS26) requires an energy barrier of

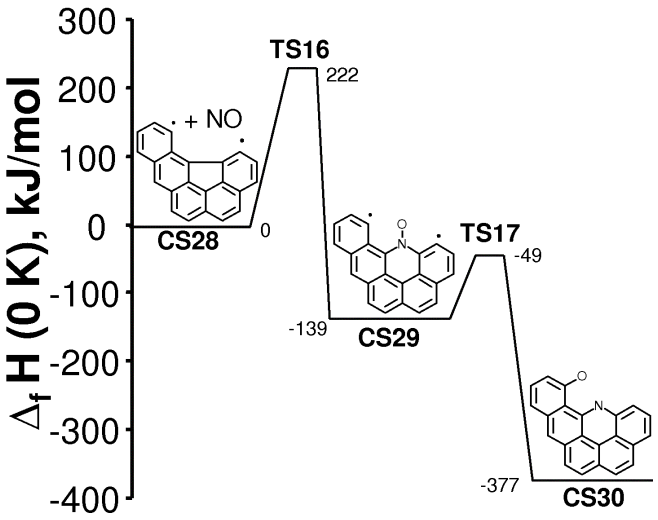

Figure 12: *Pathway 6: Potential energy diagram showing the chemisorption of* NO *molecules on a bay site of a PAH molecule, and the transfer of O atom to a nearby C atom.*

284 kJ/mol to be overcome. This branched N_2O chain can then get desorbed from the PAH. The high activation energies required in this pathway makes it difficult to occur at low temperatures, as will be shown later in this paper.

3.1.6 Pathway 6

It was found from the kMC simulations in [39] that CO removal from soot surface creates a number of bay sites. These sites may be occupied by NO molecules. Pathway 6, as shown in Figure 12, involves the addition of NO at bay sites. To study this pathway, indeno[1,2,3,4-pqra]tetraphene with two radical C atoms (CS28) was chosen as the model molecule. It can be seen in Figure 12 that the first step of NO chemisorption requires a very high energy barrier of 222 kJ/mol to be overcome indicating that the reaction would mainly take place at high temperatures. After the addition of NO on PAH, the O atom can get transferred to a nearby carbon radical, thus creating an embedded N atom in a 6-member ring. This O-transfer reaction is highly exothermic with a reaction energy of 238 kJ/mol. The transferred O atom can cause the removal of a CO molecule.

3.1.7 Pathway 7

It has been shown in pathway 6 that embedded N atoms in a six member ring can get formed through the chemisorption of NO molecules at bay sites. Another reaction that can lead to the formation of embedded N atoms is shown in Figure 13. In [27], the vertical addition of NO on a PAH was studied leading to the desorption of N_2O. However, after the addition of NO on PAH, several possibilities can arise. These possibilities or routes have been studied in pathway 7, as shown in Figure 14. Specifically, the reactions leading

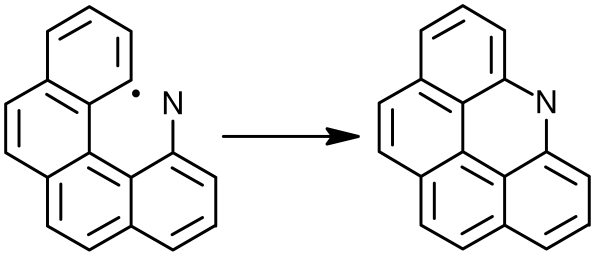

Figure 13: *Formation of an embedded N atom from a surface N atom in the bay region of a PAH molecule.*

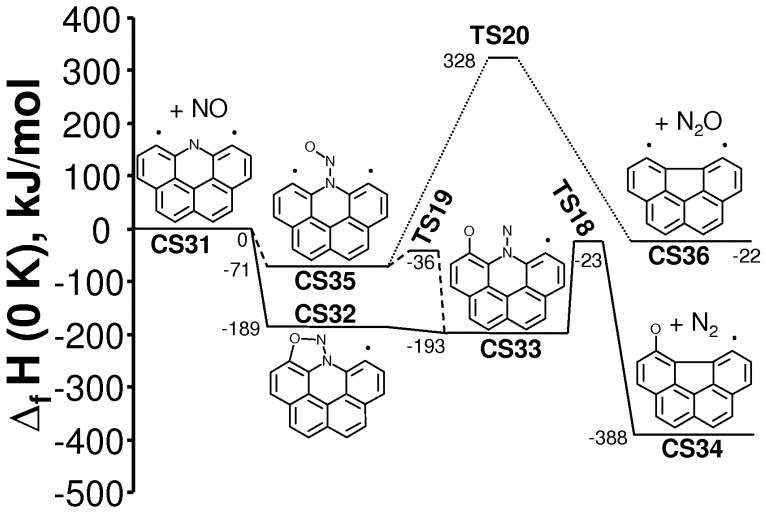

Figure 14: *Pathway 7: Potential energy diagram showing the reactivity of embedded N atoms involved in the formation of 6-member rings on PAHs towards* NO *molecules. The low energy barriers involved in this pathway (except for* $\mathrm{N_2O}$ *removal) indicate that embedded N atoms can be removed in the form of* $\mathrm{N_2}$ *at low temperatures.*

to the removal of embedded N atoms through the formation of $\mathrm{N_2}$ or $\mathrm{N_2O}$ were explored. Benzo[c]phenanthrene with an embedded N atom in the bay region and two radical C atoms (CS31) was used as the model molecule. In this case, chemisorption of NO leads to the formation of two types of chemical species depending upon the orientation of the NO molecule. The vertical addition of NO on PAH forms CS35, and parallel addition of NO to the reactive site forms CS32. Out of these two chemical species, CS32 is more stable due to the higher reaction energy involved in its formation, as can be seen in Figure 14. After the formation of CS32, similar to pathway 1, the N-O bond can break to form CS33. This breakage leads to the formation of an $\mathrm{N_2}$ chain on PAH (CS34), with one N embedded in the PAH molecule. Such an embedded $\mathrm{N_2}$ chain is stable, as its removal requires an energy barrier of 170 kJ/mol to be overcome. The vertical addition of NO on CS31 leads to the formation of CS35 (as denoted by broken lines). After CS35 is formed, there are two possible routes: O-transfer to a nearby C atom (CS33), or removal of $\mathrm{N_2O}$ (CS36).

The chemical species CS33 is more likely to form over CS36 at low temperatures due to a low energy barrier of 35 kJ/mol. After the formation of CS33, the N_2 molecule can get desorbed.

3.2 Reaction rates

The rate constants of the elementary reactions involved in the new proposed pathways are listed in table 1.

Table 1: *Elementary reaction rate constants in the form:* $\mathrm{AT^n \exp(-E/RT)}$. *The units are* $kcal$, K, mol, cm *and* sec. p.w. *represents the rate constants calculated in the present work using B3LYP/6-311++G(d,p).*

No.	Reaction	A	n	E	Ref.
Pathway 1					
1	$CS1 + 2NO \rightarrow CS2$	Infinitely fast			[39]
2	$CS2 \rightarrow CS3$	2.20×10^{13}	0.340	30.5	[39]
3	$CS3 \rightarrow CS4$	3.18×10^{08}	1.199	9.25	p.w.
-3	$CS4 \rightarrow CS3$	3.79×10^{07}	1.571	59.2	p.w.
4	$CS4 \rightarrow CS5$	7.56×10^{07}	1.571	32.5	p.w.
-4	$CS5 \rightarrow CS4$	6.15×10^{07}	1.705	45.5	p.w.
5	$CS5 \rightarrow CS6 + N_2$	9.88×10^{07}	1.687	10.8	p.w.
-5	$CS6 + N_2 \rightarrow CS5$	2.76×10^{06}	1.673	20.9	p.w.
Pathway 2					
6	$CS7 + 2NO \rightarrow CS8$	Infinitely fast			[39]
7	$CS8 \rightarrow CS9$	2.27×10^{08}	1.908	43.1	p.w.
-7	$CS9 \rightarrow CS8$	1.06×10^{08}	1.624	45.0	p.w.
8	$CS9 \rightarrow CS10 + N_2$	1.70×10^{08}	1.877	39.8	p.w.
-8	$CS10 + N_2 \rightarrow CS9$	2.13×10^{05}	1.752	17.5	p.w.
Pathway 3					
9	$CS11 + 2NO \rightarrow CS12$	Infinitely fast			[39]
10	$CS12 \rightarrow CS13$	2.20×10^{13}	0.340	30.5	[39]
11	$CS13 \rightarrow CS14$	3.12×10^{09}	0.9588	11.5	p.w.
-11	$CS14 \rightarrow CS13$	4.36×10^{07}	1.455	51.9	p.w.
12	$CS14 \rightarrow CS15$	6.61×10^{07}	1.582	31.5	p.w.
-12	$CS15 \rightarrow CS14$	1.14×10^{09}	0.919	4.80	p.w.
13	$CS15 \rightarrow CS16 + N_2$	4.71×10^{11}	0.813	15.5	p.w.
-13	$CS16 + N_2 \rightarrow CS15$	7.86×10^{06}	1.705	16.4	p.w.
Pathway 4					
14	$CS17 + NO \rightarrow CS18$	Infinitely fast			[39]
15	$CS18 \rightarrow CS19$	9.39×10^{07}	1.796	43.85	p.w.
-15	$CS19 \rightarrow CS18$	2.73×10^{08}	1.371	3.20	p.w.
16	$CS19 \rightarrow CS20 + N_2O$	1.66×10^{08}	1.880	21.3	p.w.
-16	$CS20 + N_2O \rightarrow CS19$	9.60×10^{05}	3.625	20.2	p.w.
17	$CS18 \rightarrow CS21$	4.13×10^{06}	1.863	64.9	p.w.
-17	$CS21 \rightarrow CS18$	3.61×10^{08}	0.9758	7.10	p.w.
18	$CS21 \rightarrow CS20$	5.63×10^{08}	1.5726	14.7	p.w.
-18	$CS20 \rightarrow CS21$	2.97×10^{06}	3.4033	32.1	p.w.
19	$CS21 \rightarrow CS22$	1.88×10^{08}	1.3201	18.4	p.w.
-19	$CS22 \rightarrow CS21$	4.99×10^{06}	1.686	100.1	p.w.
20	$CS22 \rightarrow CS23 + N_2$	1.13×10^{09}	1.409	8.20	p.w.

No.	Reaction	A	n	E	Ref.
-20	$CS23 + N_2 \rightarrow CS22$	2.48×10^{06}	1.727	17.9	p.w.
Pathway 5					
21	$CS24 + NO \rightarrow CS25$	4.97×10^{05}	1.755	55.6	p.w.
-21	$CS25 \rightarrow CS24 + NO$	8.47×10^{07}	1.604	49.3	p.w.
22	$CS25 \rightarrow CS26$	3.85×10^{07}	1.620	59.2	p.w.
-22	$CS26 \rightarrow CS25$	1.33×10^{10}	0.5151	1.50	p.w.
23	$CS26 \rightarrow CS27 + N_2O$	1.06×10^{08}	1.638	14.5	p.w.
-23	$CS27 + N_2O \rightarrow CS26$	6.26×10^{05}	3.452	32.5	p.w.
Pathway 6					
24	$CS28 + NO \rightarrow CS29$	1.45×10^{05}	1.826	56.75	p.w.
-24	$CS29 \rightarrow CS28 + NO$	4.51×10^{07}	1.694	77.1	p.w.
25	$CS29 \rightarrow CS30$	7.12×10^{07}	1.340	18.5	p.w.
-25	$CS30 \rightarrow CS29$	5.82×10^{06}	1.436	70.0	p.w.
Pathway 7					
26	$CS31 + NO \rightarrow CS32$	Infinitely fast			[39]
27	$CS32 \rightarrow CS33$	2.20×10^{13}	0.340	30.5	[39]
28	$CS33 \rightarrow CS34$	4.19×10^{08}	2.086	34.5	p.w.
-28	$CS34 \rightarrow CS33$	4.42×10^{07}	1.716	90.5	p.w.
29	$CS31 + NO \rightarrow CS35$	Infinitely fast			[39]
30	$CS35 \rightarrow CS33$	5.37×10^{08}	1.012	6.10	p.w.
-30	$CS33 \rightarrow CS35$	5.69×10^{08}	1.033	32.5	p.w.
31	$CS35 \rightarrow CS36 + N_2O$	3.41×10^{08}	2.052	52.4	p.w.
-31	$CS36 + N_2O \rightarrow CS35$	4.01×10^{09}	2.928	97.3	p.w.
CO removal reaction					
32	$C_6H_5O \rightarrow C_5H_5 + CO$	7.40×10^{11}		43.9	[9]
33	$C_{18}H_8O_2 \rightarrow C_{18}H_8O + CO$	5.75×10^{15}		102.4	[42]
34	$C_{14}H_7O \rightarrow C_{13}H_7 + CO$	6.83×10^{17}		105.9	p.w.

It is worth mentioning that the Wigner correction factor varied between 1.5 and 1 in the temperature range of 300-3000 K for all the reactions, and it remained close to 1 for T $>$ 1000 K. The rate constants for some of the elementary reactions not studied in this work were taken from the literature (these are also provided in table 1). One of the principal steps in all the pathways is the removal of CO molecules from PAHs. In [9], the rate constant for the reaction $C_6H_5O \rightarrow C_5H_5$+CO (also shown in figure 15a) was determined through a shock tube experiment on phenyl oxidation in the temperature range of 900–1800 K. The rate constants measured in this work are readily used in soot growth models [52, 53]. Recently, Sendt *et al.* [41, 42] studied the oxidation of PAHs by O_2 in detail using B3LYP/6-31G(d) level of theory, and theoretically evaluated the rate constant for the removal of CO from a model PAH molecule, as shown in figure 15b. The rate constant proposed in [41] is much lower than the one proposed in [9]. Due to this discrepancy in the literature, the rate for CO removal was evaluated in this work. Figure 16 provides the comparison between the rate constants for this reaction from the literature and the rate constant evaluated in this work. It can be seen in this figure that the rate proposed in this work agrees more closely with the rate of Sendt *et al.* [41]. This is due to similar levels of theory used to determine the rate constants (B3LYP/6-31G(d) in [41] and B3LYP/6-311++G(d,p) in this work).

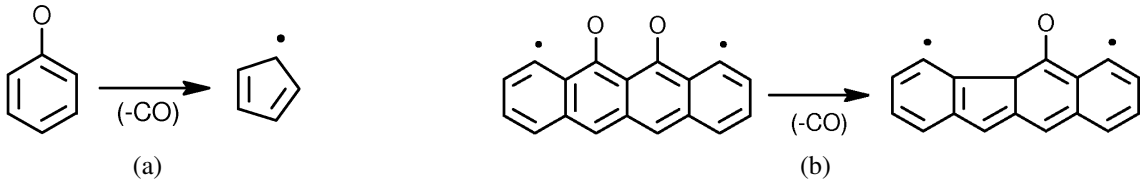

Figure 15: *(a)* CO *removal reaction studied experimentally in [9]. (b)* CO *removal reaction studied using DFT in [41].*

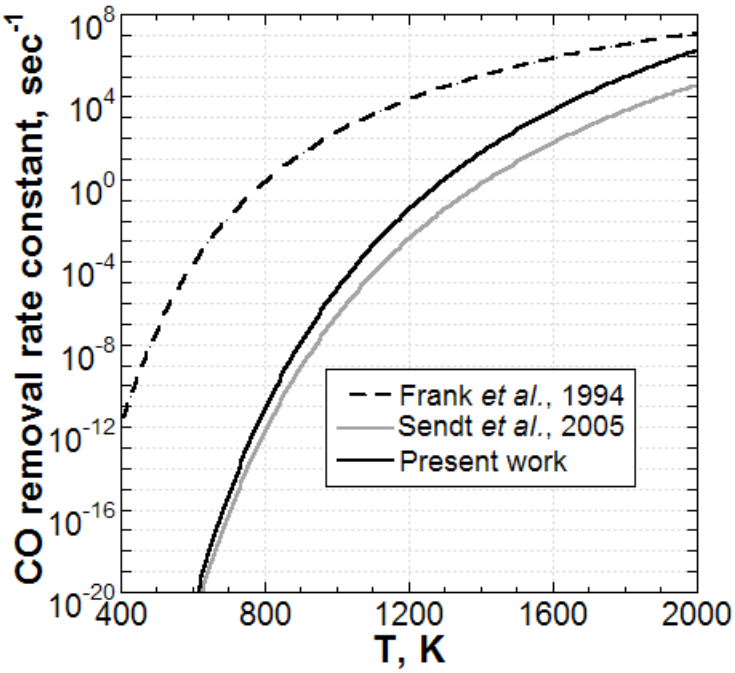

Figure 16: *Comparison of the rate constants for* CO *removal from PAHs present in the literature with the one evaluated in this work.*

3.3 kMC simulations

As mentioned in section 3.1, the KMC-ARS model was successfully applied in [39] to simulate the simultaneous reduction of PAH and NO. The reaction mechanism used in the previous work has been extended here by including the PAH reactions present in pathways 1–7. As mentioned in [39], all the PAH reactions were assumed to be irreversible. For some of the backward reactions, the concentrations of gas-phase species such as CO, N_2, and N_2O were required, which were not available. A detailed kinetic modelling of soot–NO reduction is required by using a chemical mechanism and a chemistry solver such as CHEMKIN [20] in order to determine the concentrations of the gas-phase species (for example, CO, N_2 and N_2O) formed during the reactions. Such a detailed analysis is beyond the scope of this work, as the main aim of the paper is to improve the mechanistic and fundamental understanding of the interaction between NO and soot.

With the detailed PAH–NO mechanism, the PAH model was used to study the formation of CO, N_2 and N_2O. Figure 17 shows the substrate molecules used in this work. In [39], only structure 1 was used as the substrate molecule. An example PAH in Figure 1 and the statistical study in [35] show that the PAHs comprising a soot particle can have different types of reactive sites on it. As shown in Figure 17, structure 1 mainly involves zigzag sites, structure 2 consists of zigzag and armchairs sites and structure 3 consists of zigzag, armchair and bay sites on its edge. The simulation results shown in this paper were obtained for all the three substrate structures. The simulations were carried out in two different NO–environments: Environment 1 [56] – NO concentration was kept constant at 1500 ppm, and the temperature was varied between 300°C and 900°C linearly at the rate of 5°C/min. Therefore, the total reaction time was 120 min; Environment 2 [6] – NO concentration was taken to be 500 ppm, and the temperature was held constant (isothermal conditions). The simulations were carried out at 4 different temperatures: 650°C, 750°C, 850°C and 950°C in order to study the effect of temperature on the PAH oxidation rate, and the formation of the major product species CO and N_2. All the simulation results presented in this paper were evaluated using all the three substrate molecules. For each substrate, 300 simulation runs were carried out. If not mentioned, the presented results were obtained by taking an average over the simulation results obtained for all the substrate molecules. In all the cases studied here, simulation was found to stop after some time. An attempt has been made to identify the molecular functional groups present on the final PAH structures that prevent the further oxidation of PAHs.

3.3.1 CO desorption rate

As shown in the previous section, three different rate constant are available for the desorption of CO from the PAHs. In [56], temperature programmed reaction between carbon black and NO in the absence of O_2 was carried out at a heating rate of 5°C/min (NO–environment 1 in section 3.3). It was observed that CO removal took place from the soot surface only after the temperature increased above 873 K (600°C). This information was used to choose a rate constant among the three, as described below. The kMC simulations were carried out in the NO–environment 1 on the three substrate molecules using the three proposed rate constants. Figure 18 shows the variation in the fraction of NO converted

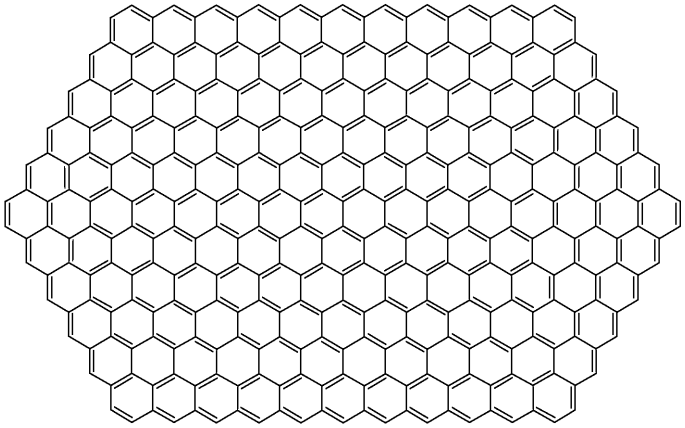

(a) Structure 1

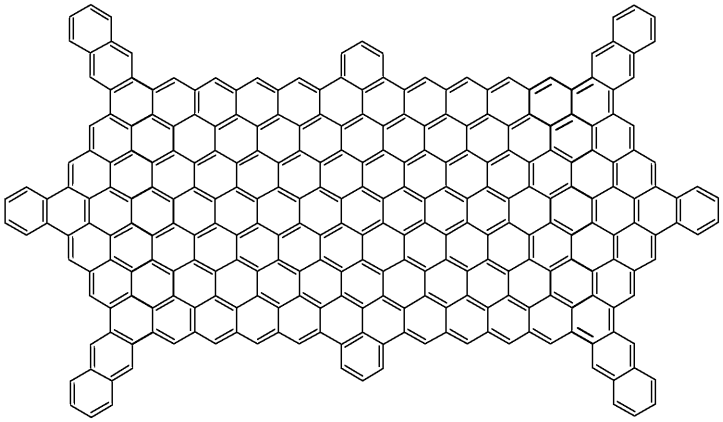

(b) Structure 2

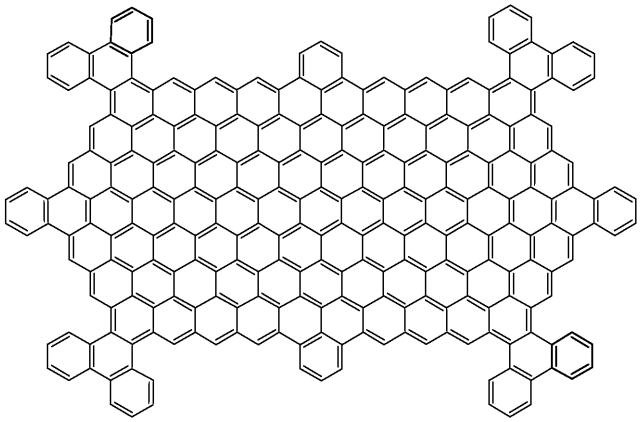

(c) Structure 3

Figure 17: *Substrate PAH structures with different numbers of reactive sites (armchairs (AC) and zigzags (ZZ) and bays (BY)) to study soot–*NO *interaction. Number of sites of type* $\mathrm{x} = \mathrm{N_x}$. *(a)* $\mathrm{N_{ZZ}} = 40,\ \mathrm{N_{AC}} = \mathrm{N_{BY}} = 0$. *(b)* $\mathrm{N_{ZZ}} = 24,\ \mathrm{N_{AC}} = 16,\ \mathrm{N_{BY}} = 0$. *(c)* $\mathrm{N_{ZZ}} = \mathrm{N_{AC}} = 12,\ \mathrm{N_{BY}} = 8$.

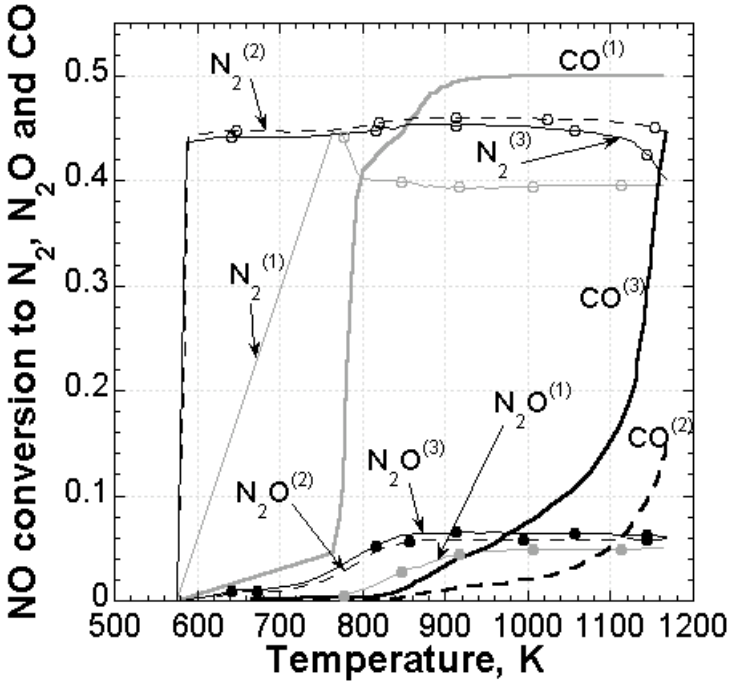

Figure 18: *Fraction of* NO *chemisorbed on PAHs converted to* CO, N_2 *and* N_2O. *The species profiles with superscript (1) were obtained with the rate constant for* CO *removal proposed by Frank et al. [9], those with superscript (2) were obtained with the rate constant proposed by Sendt et al. [40], and those with superscript (3) were obtained with the rate constant proposed in this work.*

to N_2, N_2O and CO with temperature, and with different rate constants for CO removal. This fraction X_m was calculated as: $X_m = 2 \times N_m/N_{NO}$, where N_m is the average number of molecule m released from PAHs, N_{NO} is the average number of NO molecules chemisorbed on PAHs, and m is N_2 or N_2O. For CO molecules, $X_{CO} = N_{CO}/N_{NO}$ (as only one NO is involved in producing a CO molecule). It can be seen in Figure 18 that with the CO desorption rate given in [9], CO formation starts taking place at a temperature below 600 K, while with the other rate constants, CO removal does not take place before 800 K. Figure 19 shows the temperatures at which the formation of CO starts taking place with the three different rate constants, and their comparison with the experimentally observed value. With the rate constant proposed in [40], CO removal from PAHs started at around 840 K. This value agrees reasonably well with experiments, but the amount of CO removed was very low (figure 18). In [56], in 120 minutes of reaction time, NO concentration in the gas-phase decreased by about 500 ppm, and about 400 ppm of CO were produced. This gives an approximate amount of the NO molecules converted to CO as 80%. However, with this rate, only about 15% of the NO molecules chemisorbed on PAHs were converted to CO in 120 minutes. The rate constant evaluated in this work is slightly higher than the rate of [40]. With this rate, CO desorption started taking place at around 820 K, which is reasonably close to the experimental value. The slight difference can be due to the model assumption of irreversibility of the PAH reactions. Also, at the end of

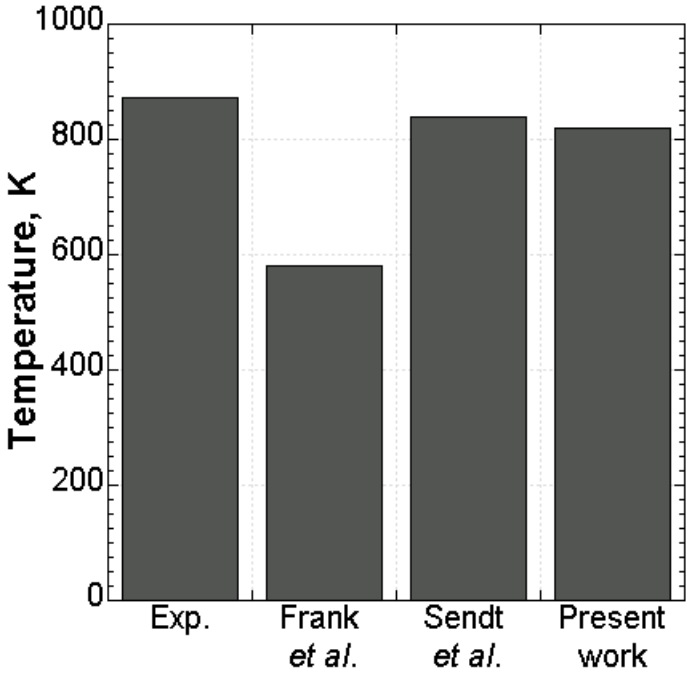

Figure 19: *Comparison of the temperature at which the desorption of* CO *molecules from soot starts taking place in experiments in* NO*–environment 1 [56] with the temperatures obtained through kMC simulations with different rates for* CO *removal. Frank et al.: Temperature for CO removal obtained with the rate constant of Frank et al. [9]. Sendt et al.: Temperature obtained with the rate constant of Sendt et al. [40]. Present work: Temperature obtained with the rate constant proposed in this work.*

120 minutes of simulation time, around 45% of the adsorbed NO got converted to CO, which is closer to the experimentally observed fraction than the previous case. The rate constant for the chemisorption of NO molecule at some of the reactive sites on PAHs were assumed to be infinitely fast (see table 1), as transition state could not be found in those cases [39]. Due to this, substrate molecules get covered with NO molecules in around 0.1 sec. Since the rates for the reactions involving N atoms are very fast, the removal of N_2 and N_2O from PAHs starts taking place at low temperature. This may not happen in practical conditions, and therefore the temperature at which the formation of N_2 starts cannot be compared to the experiments. At the end of 120 minutes, the fraction of NO converted to N_2 was around 65% in experiments, and around 40% in simulations. Section 3.3.2 lists some of the possible reasons behind the under-prediction in the conversions of NO to N_2 and CO found in the simulations. As observed in experiments [6, 43], the formation of N_2 and N_2O takes place simultaneously. Out of the three routes suggested in this work for the formation of N_2O on soot surface (in pathways 4, 5 and 7), only the ones suggested in pathways 4 and 7 led to N_2O formation at low temperatures.

It is evident from the simulation results shown above that the rate constant for CO desorption reaction proposed in this work predicts the experimental results better than the rate constants present in the literature. Therefore, the simulation results shown in the rest of this paper were evaluated with the new rate constant.

3.3.2 Reactive sites

It is shown experimentally in [57] that the reactivity of soot towards NO depends strongly on their internal structure. In their study, four carbonaceous materials–carbon black, activated carbon, fullerene black and graphite were oxidised using NO. Qualitatively, similar trends were shown by all the materials. However, an appreciable variation in the amount of NO converted on soot surface was observed. There may be various reasons behind it such as the difference in the structural arrangement of PAHs in soot, difference in the reactive sites present on the PAHs and the difference in the amount of impurities present in the particles. Since, in this work, single PAH molecules were used to study soot–NO interaction, the effect of internal structural variation cannot be studied. However, the effect of the change in reactive sites on PAHs can be studied with the PAH model. The kMC simulations were carried out in NO–environment 1 on the three structures shown in Figure 17 individually. Figure 20 shows the change in the fraction of NO converted to N_2 and CO with the change in reactive sites on PAHs. The highest conversion was found with structure 1 and the lowest with structure 3. Clearly, the stability of NO on armchair sites and the lower reactivity of NO towards bay sites makes structure 3 least desirable for NO conversion. The zigzag sites show maximum reactivity towards NO molecules. Figure 21 shows the quantitative comparison of the conversion of NO molecule chemisorbed on different PAH substrates to CO and N_2 with the experimental findings in NO–environment 1 (as mentioned in section 3.3.1). It can be seen in this figure that the conversion of NO to CO and N_2 in the simulations on structure 1 were closer to the experimental observations than the other cases. The change in the fraction of NO converted to CO and N_2 with the change in site types on PAHs can be one of the reasons for their under-prediction in the previous section, if the soot samples used in experiments in [56] were rich in zigzag

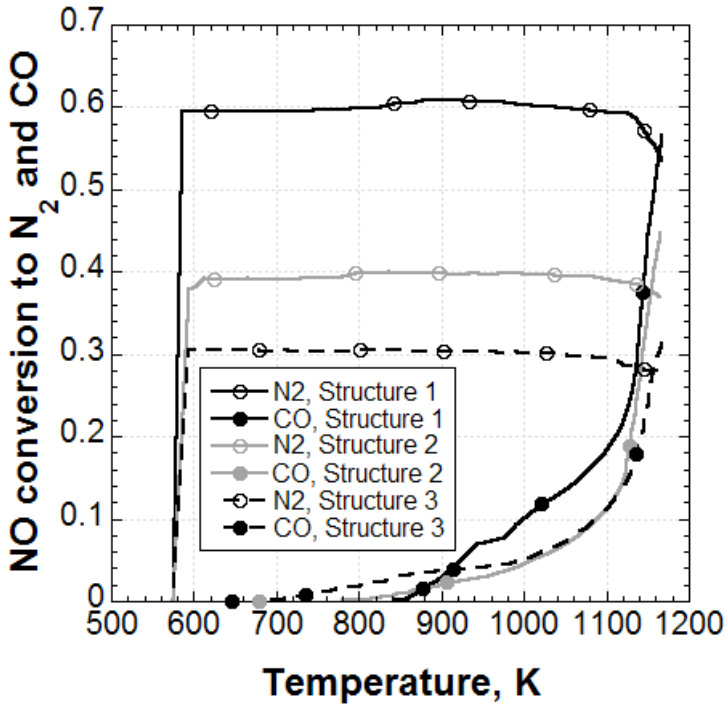

Figure 20: *Effect of the presence of different types of reactive sites on a PAH molecule. The presence of armchair and bay sites on a PAH molecule causes a decrease in the formation of* CO*. This is due to the formation of a very stable functional group when NO gets chemisorbed on armchair sites, and low reactivity of* NO *towards bay sites at low temperatures.*

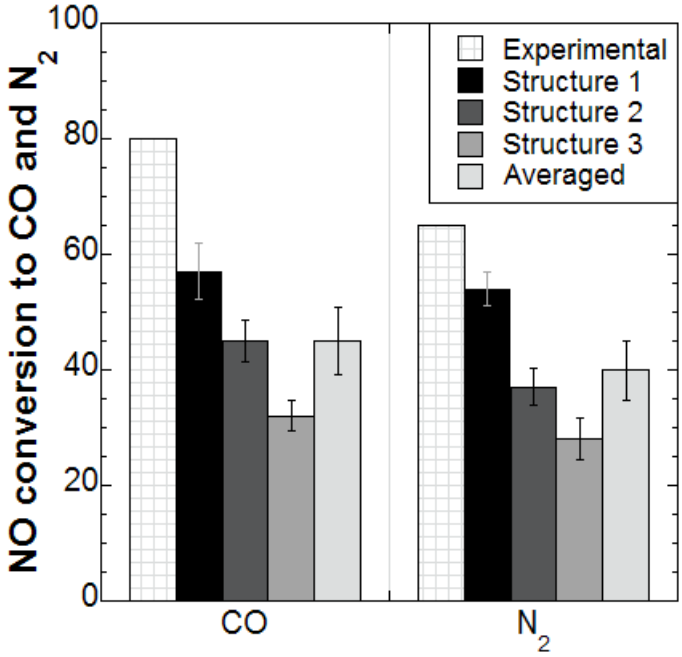

Figure 21: *Comparison of the experimentally observed conversion of* NO *to* CO *and* $\mathrm{N_2}$ *with the simulation results obtained for different substrate PAH molecules. The first stack represents the experimental results observed in [56]. The stacks 2–4 represent the simulation results obtained on the substrate structures 1–3, respectively. The fifth stack represents the simulation results averaged over the three substrate structures. The error bars show the confidence interval of 99.9% on the computed mean values.*

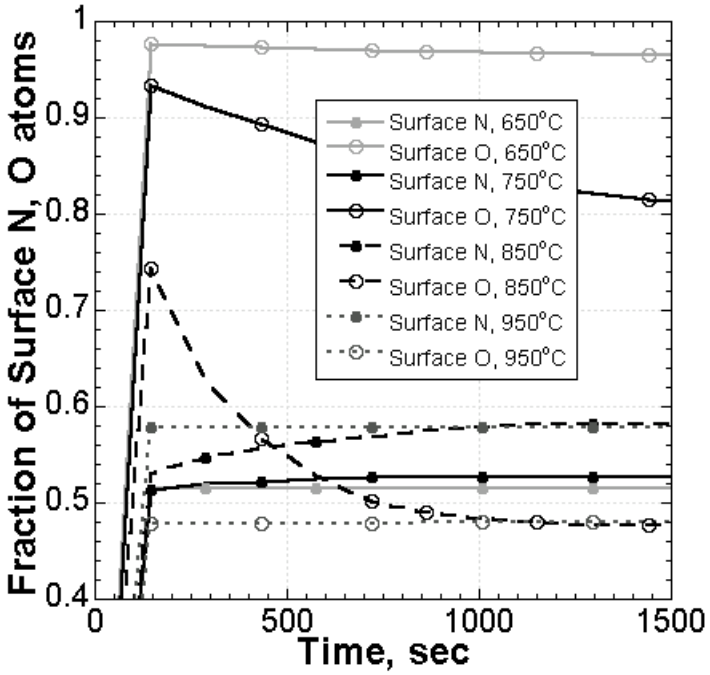

Figure 22: *Number fraction of N and O atoms present on PAH surface at different times and temperatures (the number fractions were calculated as the ratio of the number of surface atoms to the number of* NO *molecules added). The increase in temperature causes number fraction of O atoms to decrease due to increase in* CO *removal from PAHs, and number fraction of N atoms to increase due to increase in the formation of stable C-N complexes such as* NO *at bay sites.*

sites. For all types of reactive site, formation of N_2 took place before the formation of CO, which is in agreement with the experimental observations [56]. The presence of N and O atoms on soot particles from before the start of the experiments (as impurities) may also explain the model under-prediction. Another reason for this under-prediction may be the use of incomplete mechanism for the simulations. For example, no reactions are present in the mechanism for the formation of CO_2, which is observed in experiments. This highlights the possibility of the further extension of this mechanism.

3.3.3 Temperature effects

In [6], the effect of temperature on the formation of CO and N_2 was studied experimentally in NO–environment 2 (isothermal conditions). It was observed that with increasing temperature, the number of O atoms remaining on soot surface decreased, and the number of N atoms increased for a given reaction time. In this work, the number fractions of N and O atoms present on the PAH were tracked in the kMC simulations at four different temperatures (650°C, 750°C, 850°C and 950°C), and are shown in Figure 22. The number fraction for surface atoms X_{SA} were evaluated as $X_{SA} = N_{SA}/N_{NO}$, where N_{SA} is the average number of surface atoms, N_{NO} is the average number of NO molecules adsorbed

on the PAHs. It can be seen in this figure that the simulation results are qualitatively in agreement with the experimental results. In this case, quantitative comparison cannot be carried out due to the absence of information about the adsorbed NO molecules on the soot surface in experiments. At all the temperatures studied, the number fraction of N atoms remaining on the PAH varied within a small range of 0.5 to 0.6, i.e. around 50-60% of N atoms from NO remained on the PAH. This agrees reasonably well with the measurements of Reichert *et al.* [38], where 40-63% of N atoms were found to remain on the soot surface in soot–NO experiments. In Figure 22, a significant change in the number fraction of O atoms, and a noticeable change in the number fraction of N atoms on the PAH were obtained with increase in the temperature from 650°C to 950°C. This indicates that some of the reactions in the chemical mechanism become active only at high temperatures. This is also evident from Figure 23, in which the computed PAH structures at two different temperatures after a simulation time of 120 mins are shown. At 650°C, the PAH structure is covered with O atoms, as CO desorption does not take place very often at this temperature. After some reaction time, the soot–NO reaction stops due to the formation of functional groups which are very stable such as embedded N and NO, and the absence of sites available near the reactive atoms such as surface N atoms for NO addition. At this temperature, there were five main functional groups, as shown inside grey circles and numbered in Figure 23a, that prevented further addition of NO on PAH – 1) six-member NO ring; 2) embedded N atom in a 5-member ring; 3) surface N atom; 4) surface O atom; 5) bay site. With increase in temperature, the computed PAH structure changed significantly. Figure 23b shows the functional groups present on PAHs at 950°C inside grey circles, which were responsible for the reduced reactivity of soot – 1) six-member NO ring; 2) embedded N atom in a 5-member ring; 3) embedded NO in bay sites; 4) surface O atom; 5) embedded N atom in a 6-member ring; 6) surface N atom; 7) bay site. At all the temperatures, some of the surface N atoms were found to be non-reactive due to the absence of nearby reactive sites to aid the further addition of NO molecules. At 950°C, the amount of surface O atoms were much less than their amount at 650°C due to the increase in PAH oxidation rate through CO removal. This is evident from Figure 24. With increase in temperature, the initial rate of carbon oxidation increases. At 650° and 750°, the rate of oxidation is very slow. However, at higher temperatures, most of the O atoms present on the PAH are removed through the formation of CO in less than 2000 s. The oxidation rate decreases with time as the number of removable O atoms decreases. For example, the O atoms present in the embedded NO on a bay site or in a 6-member NO ring are difficult to remove even at high temperatures (when none of the reactions proposed in pathways 2 and 3 on 6-member NO rings can take place due to the absence of nearby NO rings with desired orientations for further reactions). The O atoms in 5-member NO rings are able to oxidise PAHs, as the N-O bond can break easily. The computed structures in Figure 23 show that the PAH becomes inactive earlier at low temperatures than at high temperatures. This is because some of the reactions present in the chemical mechanism do not take place at low temperatures, even if the reactive sites required for them to take place are available. Figure 25 presents the average counts of some of the principal reactions taking place on PAHs at different temperatures. The PAH reactions corresponding to the numbers present on the X-axis in this figure are explained in the caption. The average count of N_2 molecules formed by surface N atoms on PAHs (reaction 1) do not change significantly with temperature. However, N_2 formation from embedded N atoms

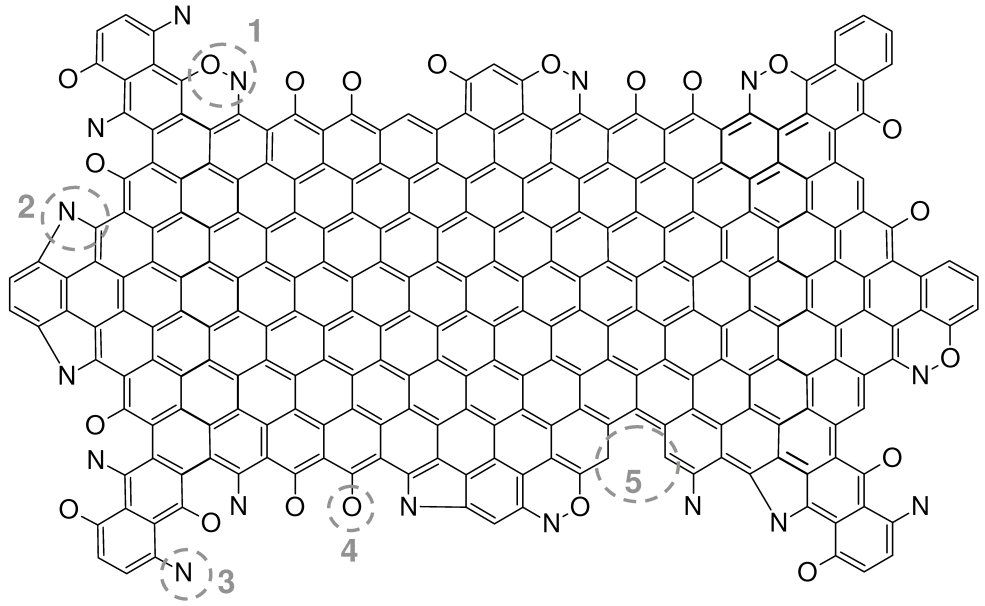

(a)

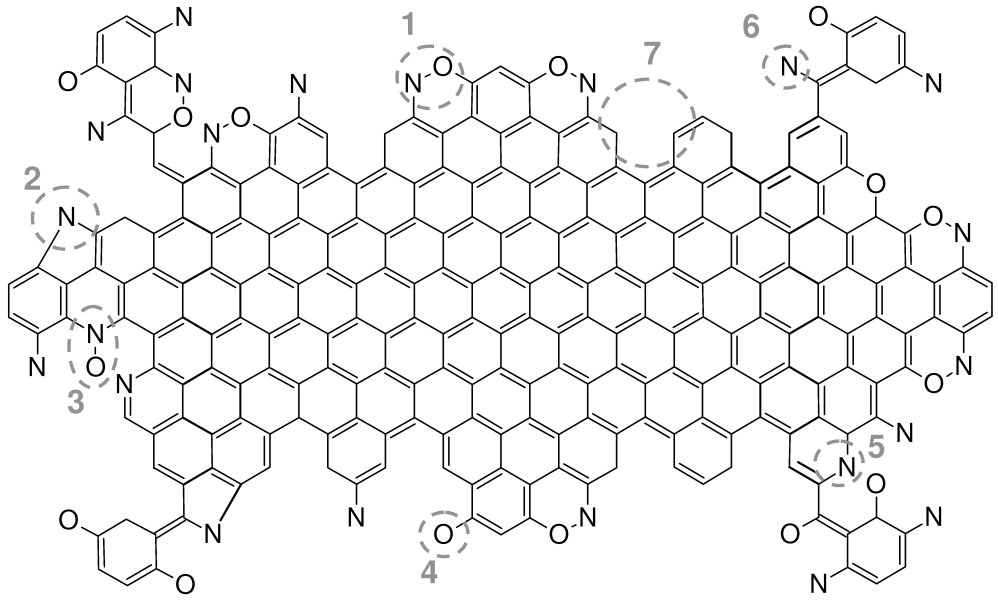

(b)

Figure 23: *Example computed PAH structures obtained at time, t = 7200 sec in isothermal conditions, when the concentration of* NO *was 500 ppm. (a) Temperature = 650°C, (b) Temperature = 950°C. Structure 2 (Figure 17) was chosen as the substrate PAH structure for simulation at both the temperatures. The functional groups which were responsible for the reduced reactivity of PAHS at two different temperatures are shown inside grey circles.*

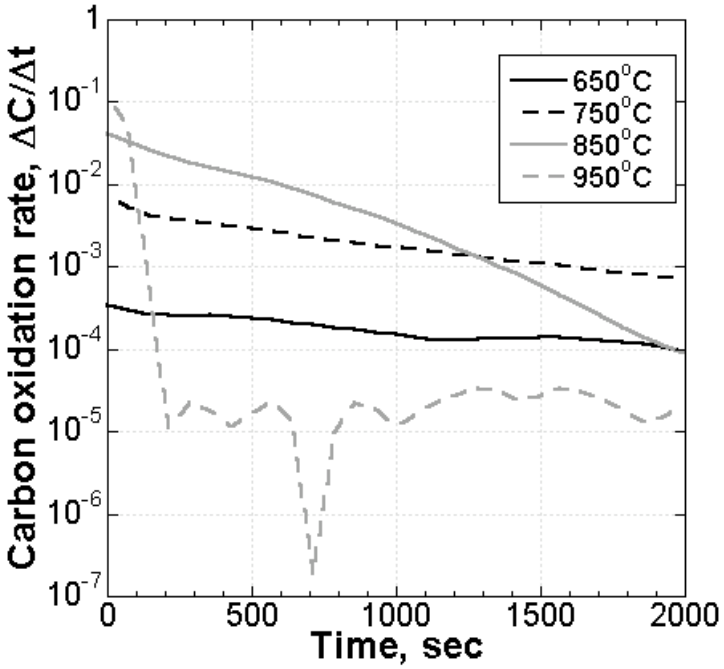

Figure 24: *Oxidation rate of carbon atoms present in PAHs at different temperatures, calculated as the change in C atom count per unit change in time ($\frac{\triangle C}{\triangle t}$). A significant increase in the oxidation rate was observed when the temperature increased from 650^o to 950^o.*

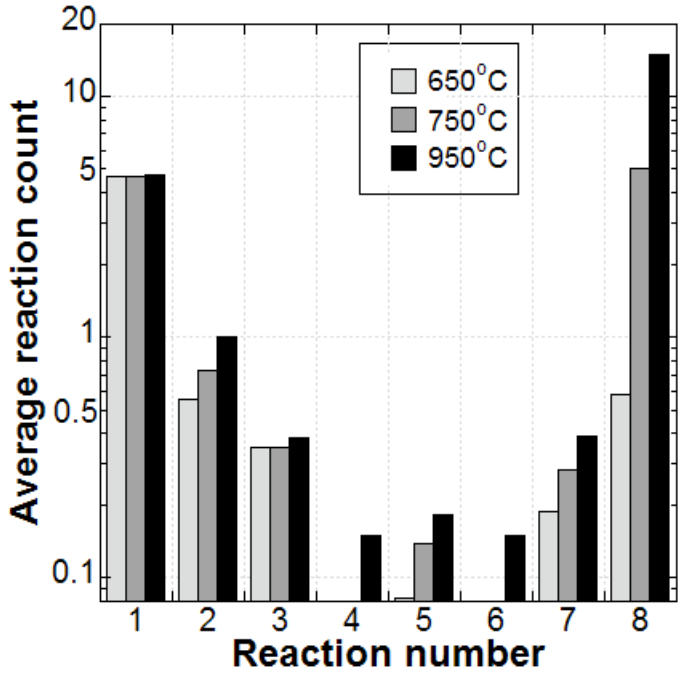

Figure 25: *Average counts of some of the principal reactions that took place on PAHs. Reaction 1 – total* N_2 *removal from surface N atoms (mechanisms 1–3 and those proposed in [39]); Reaction 2 –* N_2 *removal from embedded N atoms (mechanism 7); Reaction 3 –* N_2O *removal via mechanism 4; Reaction 4 –* N_2O *removal via mechanism 5; Reaction 5 –* N_2O *removal via mechanism 7; Reaction 6 – embedded* NO *formation via mechanism 6; Reaction 7 – O transfer on PAH via mechanism 7; Reaction 8 – total* CO *removal. The formation of* N_2 *and* CO *dominates at all the temperatures.*

increases with increasing temperature (reaction 2). Similar behaviour is shown by N_2O. Their formation from surface N does not change significantly with temperature (reaction 3). However, N_2O formation through reaction 4 takes place only at 950°C. This shows that the functional group, embedded N atom in a 5-member ring is very stable, and is only reactive at very high temperatures. N_2O formation from embedded N atoms in 6-member rings increases with temperature (reaction 5). The bay sites on PAHs form very frequently with the removal of CO molecules. However, these sites are only reactive at high temperatures (> 750°C). If NO is added vertically on the soot surface (as shown in pathway 7), the O atom of NO is able to get transferred to nearby C atoms. The number of such O transfers increase with temperature (reaction 7). As indicated previously, CO removal depends strongly on temperature (reaction 8), and the oxidation of PAHs mainly takes place at high temperatures (> 650°C).

It is clear that the temperature significantly affects the amount of NO converted to CO and N_2 on soot surface. Some of the PAH reactions, which are not active at low temperatures, can take place at high temperatures. With the present reaction mechanism, whilst a satisfactory agreement between experimental and simulation results was obtained, it is possible to further improve this match through mechanism extension by including new reactions for the formation of CO_2, CO and N_2.

4 Conclusion

A theoretical study on the interaction between soot and NO molecules in the absence of oxygen has been carried out in order to develop the mechanistic understanding behind the formation of chemical species such as CO, N_2 and N_2O on soot. Seven different reaction pathways on PAH molecules have been presented. These reactions take place on different types of reactive sites such as armchair sites, bay sites, and embedded and surface N radicals. The energetics and kinetics of the PAH reactions were evaluated using density functional theory and transition state theory, respectively. The chemisorption of NO on PAHs was found to be exothermic irrespective of their relative orientations considered in this work. The formation of N_2 on PAHs involved low energy barriers indicating that it can form at low temperatures as observed experimentally. A new rate for the removal of CO from PAHs was proposed due to a discrepancy in the rates present in the literature. A PAH growth model, called the kinetic Monte Carlo–Aromatic Site (KMC-ARS) model has been used to simulate the formation of gas-phase species on PAHs by using the reactions proposed in this work appended with the reactions listed in [39]. This combination of a mechanistic DFT study and a kMC study has enabled a qualitative, and to some extent, quantitative description of the experimental results on the simultaneous reduction of soot and NO. The model predicts the formation of CO, as observed experimentally in a soot–NO environment, at temperatures > 600°C in substantial amount with the rate proposed in this work. The observed experimental trends in isothermal conditions that the amount of N atoms present on soot surface increases and the the amount of O atoms decreases with increasing temperature, have been successfully captured in the simulations. Furthermore, it was observed in [38] that 40-63 % of N atoms remained on soot surface after soot–NO reaction, which agrees reasonably well with the model prediction of 50-60%. The amount

of CO and N_2 formed in the reactions were slightly under-predicted. There are many possible reasons behind this such as the presence of N and O atoms as impurities in soot, the presence of highly reactive sites such as zigzags leading to the faster conversion of NO to CO and N_2 or an incomplete reaction mechanism. Therefore, further development of the mechanism is required. The computed PAH structures at different temperatures were also analysed to gain information about the functional groups that are responsible for site blockage on soot leading to their reduced reactivity with increasing time. As proposed in the literature, some of the functional groups of N and O atoms along with bay sites were found to be very stable at low temperatures, and were reactive mainly at high temperatures ($\approx 950^{o}$C). Also, the reactive atoms such as surface N atoms were not able to react further due to the absence of suitable reactive sites nearby for further addition of NO. The functional groups reducing soot reactivity at low temperatures differed from those present at high temperatures.

Acknowledgement

A.R. is grateful to Cambridge Commonwealth Trusts (CCT) and Clare College, Cambridge for their financial support. The authors highly acknowledge the support of EPSRC under EP/C547241/1 and EP/E01724X/1.

References

[1] I. Aarna and E. M. Suuberg. A review of the kinetics of the nitric oxide-carbon reaction. *Fuel*, 76:475–491, 1997.

[2] D. L. Baulch, C. T. Bowman, C. J. Cobos, R. A. Cox, T. Just, J. A. Kerr, M. J. Pilling, D. Stocker, J. Troe, W. Tsang, R. W. Walker, and J. Warnatz. Evaluated Kinetic Data for Combustion Modeling: Supplement II. *J. Phys. Chem. Ref. Data*, 34:757–1397, 2005.

[3] J. S. Beckman and W. H. Koppenol. Nitric oxide, superoxide, and peroxynitrite: the good, the bad, and ugly. *Am. J. Physiol.*, 271:1424–1437, 1997.

[4] R. L. Bell and T. N. Truong. Direct ab initio dynamics studies of proton transfer in hydrogen-bond systems. *J. Chem. Phys.*, 101:10442–10451, 1994.

[5] A. Boyano, M. E. Gálvez, M. J. Lázaro, and R. Moliner. Characterization and kinetic study of carbon-based briquettes for the reduction of NO. *Carbon*, 44:2399–2403, 2006.

[6] P. Chambrion, T. Kyotani, and A. Tomita. Role of N-containing surface species on no reduction by carbon. *Energ. Fuel*, 12(5):469–476, 1998.

[7] P. Chambrion, T. Kyotani, and A. Tomita. C-NO reaction in the presence of O_2. *Proc. Combust. Inst.*, 27:3053–3059, 1998.

[8] H. X. Chen and R. A. Dobbins. Crystallogenesis of Particles Formed in Hydrocarbon Combustion. *Combust. Sci. Technol.*, 159:109–128, 2000. doi:10.1080/00102200008935779.

[9] P. Frank, J. Herzler, T. Just, and C. Wahl. High-temperature reactions of phenyl oxidation. *Proc. Combust. Inst.*, 25:833–840, 1994.

[10] M. J. Frisch, G. W. Trucks, H. B. Schlegel, G. E. Scuseria, M. A. Robb, J. R. Cheeseman, J. A. Montgomery, Jr., T. Vreven, K. N. Kudin, J. C. Burant, J. M. Millam, S. S. Iyengar, J. Tomasi, V. Barone, B. Mennucci, M. Cossi, G. Scalmani, N. Rega, G. A. Petersson, H. Nakatsuji, M. Hada, M. Ehara, K. Toyota, R. Fukuda, J. Hasegawa, M. Ishida, T. Nakajima, Y. Honda, O. Kitao, H. Nakai, M. Klene, X. Li, J. E. Knox, H. P. Hratchian, J. B. Cross, V. Bakken, C. Adamo, J. Jaramillo, R. Gomperts, R. E. Stratmann, O. Yazyev, A. J. Austin, R. Cammi, C. Pomelli, J. W. Ochterski, P. Y. Ayala, K. Morokuma, G. A. Voth, P. Salvador, J. J. Dannenberg, V. G. Zakrzewski, S. Dapprich, A. D. Daniels, M. C. Strain, O. Farkas, D. K. Malick, A. D. Rabuck, K. Raghavachari, J. B. Foresman, J. V. Ortiz, Q. Cui, A. G. Baboul, S. Clifford, J. Cioslowski, B. B. Stefanov, G. Liu, A. Liashenko, P. Piskorz, I. Komaromi, R. L. Martin, D. J. Fox, T. Keith, M. A. Al-Laham, C. Y. Peng, A. Nanayakkara, M. Challacombe, P. M. W. Gill, B. Johnson, W. Chen, M. W. Wong, C. Gonzalez, , and J. A. Pople. *Gaussian 03*, Revision E.01; Gaussian, Inc., Wallingford CT. 2004.

[11] A. G-Lafont, T. N. Truong, and D. G. Truhlar. Direct Dynamics Calculations with Neglect of Diatomic Differential Overlap Molecular Orbltai Theory with Specific Reaction Parameters. *J. Phys. Chem.*, 95:4618–4627, 1991.

[12] M. J. Illán-Gómez, A. Linares-Solano, L. R. Radovic, and C. S. d. Lecea. NO Reduction by Activated Carbons. 2. Catalytic Effect of Potassium. *Energ. Fuel*, 9: 97–103, 1995. doi:10.1021/ef00049a015.

[13] M. J. Illán-Gómez, A. Linares-Solano, L. R. Radovic, and C. S. d. Lecea. NO Reduction by Activated Carbons. 7. Some Mechanistic Aspects of Uncatalyzed and Catalyzed Reaction. *Energ Fuels*, 10:158–168, 1996.

[14] M. J. Illán-Gómez, A. Linares-Solano, C. S. d. Lecea, and J. M. Calo. NO Reduction by Activated Carbons. 1. the Role of Carbon Porosity and Surface Area. *Energ. Fuel*, 7:146–154, 1993. doi:10.1021/ef00037a023.

[15] T. Ishiguro, Y. Takatori, and K. Akihama. Microstructure of Diesel Soot Particles Probed by Electron Microscopy: First Observation of Inner Core and Outer Shell. *Combust. Flame*, 108:231–234, 1997. doi:10.1016/S0010-2180(96)00206-4.

[16] M. Jeguirim, V. Tschamber, J. F. Brilhac, and P. Ehrburger. Oxidation mechanism of carbon black by NO_2: Effect of water vapour. *Fuel*, 84:1949–1956, 2005. doi:10.1016/j.fuel.2005.03.026.

[17] M. Jeguirim, V. Tschamber, and J. F. Brilhac. Kinetics of catalyzed and non-catalyzed soot oxidation with nitrogen dioxide under regeneration particle trap conditions. *J. Chem. Technol. Biotechnol.*, 84:770–776, 2009. doi:10.1002/jctb.2110.

[18] J. M. Jones and D. H. Jones. Modelling the competition between annealing and oxidation in the carbonoxygen reaction. *Carbon*, 45:668–689, 2007.

[19] J. M. Jones, W. A. T. Ellyatt, F. E. Ndaji, and K. M. Thomas. Flow injection-thermal analysis-mass spectrometry: Application to studies of carbon gasification reactions. *Carbon*, 25:217–225, 1996.

[20] R. J. Kee, F. M. Ropley, E. Meeks, and J. A. Miller. CHEMKIN-III: A FORTRAN chemical kinetics package for the analysis of gas-phase chemicl and plasma kinetics. Technical Report UC-405 SAND96-8216, Sandia National Laboratories, Livermore, CA 94551-0969, USA, May 1996.

[21] V. V. Kislov, N. I. Islamova, A. M. Kolker, S. H. Lin, and A. M. Mebel. Hydrogen Abstraction Acetylene Addition and Diels-Alder Mechanisms of PAH Formation: A Detailed Study Using First Principles Calculations. *J. Chem. Theory Comput.*, 1: 908–924, 2005. doi:10.1021/ct0500491.

[22] B. C. Kone. Nitric oxide in renal health and disease. *Am. J. Kidney Dis.*, 30:311–333, 1997.

[23] B. Kumfer and I. Kennedy. *The role of soot in the health effects of inhaled airborne particles*, pages 1–15. Proceedings of an International Workshop held in Villa Orlandi, Anacapri, May 13-16, 2007. Editor: H Bockhorn, A D'Anna, A F Sarofim and H Wang. Karlsruhe University Press.

[24] N. Kunioshi, M. Touda, and S. Fukutani. Computational study on the formation of five-membered rings in pah through reaction with O_2. *Combustion and Flame*, 128: 292–300, 2002.

[25] S. Kureti, W. Weisweiler, and K. Hizbullah. Simultaneous conversion of nitrogen oxides and soot into nitrogen and carbon dioxide over iron containing oxide catalysts in diesel exhaust gas. *Appl. Catal. B-Environ.*, 43:281–291, 2003.

[26] T. Kyotani and A. Tomita. Analysis of the Reaction of Carbon with NO/N_2O Using Ab Initio Molecular Orbital Theory. *J. Phys. Chem. B*, 103:3434–3441, 1999.

[27] R. López and T. L. Sordo. A density functional theory study of N_2O formation from the reaction of NO with pyridine and with acridine. *Theor. Chem. Acc.*, 112: 270–276, 2004. doi:10.1007/s00214-004-0575-2.

[28] K. Matsuoka, T. Akahane, H. Aso, A. Sharma, and A. Tomita. The size of polyaromatic layer of coal char estimated from elemental analysis data. *Fuel*, 87:539–545, 2008.

[29] A. M. Mebel, M. C. Lin, T. Yu, and K. Morokuma. Theoretical Study of Potential Energy Surface and Thermal Rate Constants for the $C_6H_5 + H_2$ and $C_6H_6 + H$ Reactions. *J. Phys. Chem. A*, 101:3189–3196, 1997. doi:10.1021/jp9702356.

[30] A. Montoya, T. N. Truong, and A. F. Sarofim. Application of density functional theory to the study of the reaction of NO with char-bound nitrogen during combustion. *J. Phys. Chem. A*, 104:8409–8417, 2000. doi:10.1021/jp001045p.

[31] Y. Nakanishi, Y. Yoshihara, and K. Nishiwaki. Non-catalytic reduction of NO in diesel exhaust with the addition of methylamine. *Society of Automotive Engineers of Japan*, 21:561–566, 2000.

[32] N. Nejar, M. Makkee, and M. J. Illán-Gómez. Catalytic removal of NO_x and soot from diesel exhaust: Oxidation behaviour of carbon materials used as model soot. *Appl. Catal. B-Environ.*, 75:11–16, 2007.

[33] H. Orikasa, K. Matsuoka, T. Kyotani, and A. Tomita. HCN and N_2 formation mechanism during NO/char reaction. *Proc. Combust. Inst.*, 29:2283–2289, 2002.

[34] M. L. Pisarello, V. Milt, M. A. Peralta, C. A. Querini, and E. E. Miró. Simultaneous removal of soot and nitrogen oxides from diesel engine exhausts. *Catal. Today*, 75: 465–470, 2002.

[35] A. Raj, M. Celnik, R. Shirley, M. Sander, R. Patterson, R. West, and M. Kraft. A statistical approach to develop a detailed soot growth model using PAH characteristics. *Combust. Flame*, 156:896–913, 2009. doi:10.1016/j.combustflame.2009.01.005.

[36] A. Raj, P. Man, T. Totton, M. Sander, R. Shirley, and M. Kraft. New PAH processes to improve the model prediction of the composition of combustion-generated PAHs and soot. Technical Report 69, c4e Preprint-Series, Cambridge, 2009. URL http://como.cheng.cam.ac.uk. Material from this preprint has been published in [37].

[37] A. Raj, P. Man, T. Totton, M. Sander, R. Shirley, and M. Kraft. New polycyclic aromatic hydrocarbon (PAH) surface processes to improve the model prediction of the composition of combustion-generated PAHs and soot. *Carbon*, 2009. doi:10.1016/j.carbon.2009.09.030. in press.

[38] D. Reichert, H. Bockhorn, and S. Kureti. Study of the reaction of NO_x and soot on Fe_2O_3 catalyst in excess of O_2. *Appl. Catal. B-Environ.*, 80:248–259, 2008.

[39] M. Sander, A. Raj, O. Inderwildi, M. Kraft, S. Kureti, and H. Bockhorn. The simultaneous reduction of nitric oxide and soot in emissions from diesel engines. *Carbon*, 47:866–875, 2009.

[40] K. Sendt and B. S. Haynes. Density functional study of the chemisorption of O_2 on the zig-zag surface of graphite. *Combust. Flame*, 143:629–643, 2005.

[41] K. Sendt and B. S. Haynes. Density functional study of the chemisorption of O_2 on the armchair surface of graphite. *Proceedings of the Combustion Institute*, 30: 2141–2149, 2005.

[42] K. Sendt and B. S. Haynes. Density functional study of the chemisorption of O_2 on the zig-zag surface of graphite. *Combustion and Flame*, 143:629–643, 2005.

[43] W. F. Shangguan, Y. Teraoka, and S. Kagawa. Kinetics of soot-O_2, soot-NO and soot-O_2-NO reactions over spinel-type $CuFe_2O_4$ catalyst. *Appl. catal. B-Environ.*, 12:237–247, 1997.

[44] B. R. Stanmore, V. Tschamber, and J. F. Brilhac. Oxidation of carbon by NO_x, with particular reference to NO_2 and N_2O. *Fuel*, 87:131–146, 2008.

[45] B. Temelso, C. D. Sherrill, R. C. Merkle, and R. A. Freitas Jr. High-Level ab Initio Studies of Hydrogen Abstraction from Prototype Hydrocarbon Systems. *J. phys. Chem. A*, 110:11160–11173, 2006.

[46] C. J. Tighe, J. S. Dennis, A. N. Hayhurst, and M. V. Twigg. The reactions of NO with diesel soot, fullerene, carbon nanotubes and activated carbons doped with transition metal. *Proc. Combust. Inst.*, 32:1989–1996, 2009. doi:10.1016/j.proci.2008.06.165.

[47] M. V. Twigg. Progress and future challenges in controlling automotive exhaust gas emissions. *Applied Catalysis B: Environmental*, 70:2–15, 2007. doi:10.1016/j.apcatb.2006.02.029.

[48] B. V. Unterreiner, M. Sierka, and R. Ahlrichs. Reaction pathways for growth of polycyclic aromatic hydrocarbons under combustion conditions, a DFT study. *Phys. Chem. Chem. Phys.*, 6:4377–4384, 2004. doi:10.1039/b407279k.

[49] R. L. Vander Wal. A TEM Methodology for the Study of Soot Particle Structure. *Combust. Sci. Tech.*, 126:333–357, 1997. doi:10.1080/00102209708935680.

[50] R. L. Vander Wal. An Illustration of Soot Structure by Dark Field Transmission Electrom Microscopy. *Combust. Sci. Tech.*, 132:315–323, 1998. doi:10.1080/00102209808952018.

[51] R. L. Vander Wal, A. Yezerets, N. W. Currier, D. H. Kim, and C. M. Wang. HRTEM Study of diesel soot collected from diesel particulate filters. *Carbon*, 45:70–77, 2007. doi:10.1016/j.carbon.2006.08.005.

[52] A. Violi and S. Izvekov. Soot primary particle formulation from multiscale coarse-grained molecular dynamics simulation. *Proc. Combust. Inst.*, 31:529–537, 2007. doi:10.1016/j.proci.2006.07.240.

[53] H. Wang and M. Frenklach. A detailed kinetic modeling study of aromatic formation in laminar premixed acetylene and ethylene flames. *Combust. Flame*, 110:173–221, 1997. doi:10.1016/S0010-2180(97)00068-0.

[54] R. Whitesides, A. C. Kollas, D. Domin, W. A. Lester Jr, and M. Frenklach. Graphene Layer Growth: Collision of migrating five-member rings. *Proc. Combust. Inst.*, 31: 539–546, 2007.

[55] K. Yamamoto, S. Oohori, H. Yamashita, and S. Daido. Simulation on soot deposition and combustion in diesel particulate filter. *Proc. Combust. Inst.*, 32:1965–1972, 2009. doi:10.1016/j.proci.2008.06.081.

[56] J. Yang, G. Mestl, D. Herein, R. Schlögl, and J. Find. Reaction of NO with carbonaceous materials I. reaction and adsorption of NO on ashless carbon black. *Carbon*, 38:715–727, 2000.

[57] J. Yang, E. Sanchez-Cortezon, N. Pfänder, U. Wild, G. Mestl, J. Find, and R. Schlögl. Reaction of NO with carbonaceous materials: III. influence of the structure of the materials. *Carbon*, 38:2029–2039, 2000.

[58] D. C. Young. *Computational Chemistry: A Practical Guide for Applying Techniques to Real-World Problems*. John Wiley & Sons Inc., 2001.

[59] M. Zheng, G. T. Reader, and J. G. Hawley. Diesel engine exhaust gas recirculation-a review on advanced and novel concepts. *Energ. Convers. Manage.*, 45:883–900, 2004.